SWELL PREDICTION BY A MULTIPLE POINT- SOURCE SWELL GENERATION MODEL

Carl F. Kauffmann

NAVAL POSTGRADUATE SCHOOL
Monterey, California

THESIS

SWELL PREDICTION BY A MULTIPLE
POINT-SOURCE SWELL GENERATION MODEL

by

Carl F. Kauffmann

Thesis Advisor: W. C. Thompson

March 1973

SWELL PREDICTION BY A MULTIPLE POINT-SOURCE SWELL GENERATION MODEL

by

Carl F. Kauffmann
Lieutenant, United States Navy
B.S., United States Naval Academy, 1966

Submitted in partial fulfillment of the
requirements for the degree of

MASTER OF SCIENCE IN OCEANOGRAPHY

from the

NAVAL POSTGRADUATE SCHOOL
March 1973

ABSTRACT

A method was developed for forecasting swell using a spectral wave-generation model based on a multiple point-source concept of swell origin. The multiple point-source concept considers that the peak-energy swell emanating from a moving cyclonic storm can be considered to have been produced at one or more space-time point sources in the storm by the impulsive introduction of energy into the sea. The method was tested on five North Pacific storms generating swell recorded at Monterey, California. Predicted swell heights, which were made for two storms, were significantly lower than the observed heights. The time of occurrence of the predicted peak height agreed with that observed for the swell from one storm, but differed by about ten hours for the other. Predictions of the dominant swell period were accurate to within about one second over the entire range of observed periods for all storms.

TABLE OF CONTENTS

LIST OF TABLES

LIST OF ILLUSTRATIONS

I. OBJECTIVE OF THE STUDY

The objective of this study is to develop a method for forecasting swell at a single observation site based on a multiple point-source concept of swell origin and using a spectral wave generation model.

The multiple point-source concept of swell origin was proposed to this investigator by Professor Warren C. Thompson of the Department of Oceanography, Naval Postgraduate School. The concept involves the assumption that the peak-energy swell emanating from a moving cyclonic storm can be considered to have been produced at one or more space-time point sources in the storm by the impulsive introduction of energy into the sea.

The swell generation model proposed is a spectral model utilizing the Pierson-Moskowitz (1964) spectrum and assumes that the spectrum of peak-energy waves present at a point-source can be computed from the surface wind speed at that point and the speed of the storm.

The products of the method are a forecast of the dominant swell period and significant swell height with time at the forecast station.

The method was tested on five North Pacific storms and the forecast products were compared with the observed swell recorded at Monterey, California.

II. DEVELOPMENT OF THE METHOD

A. BASIC APPROACH

In a notable study of swell propagated over long distances and recorded offshore from San Clemente Island, California, Munk, et al. (1963) observed slanting ridges in the energy density topography drawn on a plot of frequency versus time. Each of these ridge lines described the frequency-time distribution of the maximum energy in a swell train arriving at the recorder site from a given storm. It was shown that a ridge line can be accounted for in terms of classical wave theory so long as the energy spectrum is assumed to have been generated at a point-source in space and time. The slope and zero-frequency intercept of a particular slanting ridge line was then used to compute the effective origin time and distance from the station to the source of the peak energy swell.

The swell prediction model developed in the present study effectively employs the reverse of the above procedure. A "point-source" is identified in the wind field of a moving cyclonic storm on each of a succession of six-hourly weather maps covering the life of the storm. Each point-source represents a potential point of origin of the dominant wave energy emerging from the storm and is considered to be located at that point where the peak winds are generating waves directly toward the distant station for which the prediction

is to be made. A wave spectrum is computed at each point-source; the characteristics of each spectrum are determined from the surface wind speed at that point and the speed of the storm toward the station. Each period component of the spectrum is propagated toward the station at a group velocity which is a function of its period. The dispersive arrival at the station of the waves propagating from a single point-source is represented by a plot of period versus time of arrival.

The energy in each spectral component of the swell train represented by a particular period-time curve is calculated by modifying the energy spectrum at the point-source for the effects of angular spreading and high-frequency attenuation. By graphing the energy-density values associated with the various period components as a function of time of arrival at the station, an energy density-time plot is obtained. This plot is termed a "propagated spectrum". The envelope of the family of propagated spectra obtained from the series of point-sources during the life of a storm represents the energy density of the spectral peaks at each arrival time at the observation station.

The total energy in the swell at any given arrival time is estimated by computing the area under the plot of frequency versus energy density values obtained from a time-cut of the propagated spectra. The predicted swell heights are assumed to be statistically related to these coarse energy calculations. The time distribution of dominant

swell periods is obtained from the time distribution of the frequency components containing the maximum energy density in the propagated spectra.

In the following sections these procedures will be described and illustrated using synoptic weather events.

B. GENERATION OF SEA SPECTRA

1. Selection of Sea-Level Pressure Charts

The weather charts used in this study were six-hourly sea-level pressure analyses of the North Pacific Ocean produced by the Fleet Numerical Weather Central (FNWC), Monterey. An advantage of using these computer-produced analyses is the objective manner in which the isobaric fields are produced. The fields analyzed covered the entire area of the North Pacific under investigation.

The weather charts were chosen on the basis of frequency-time analyses of five selected swell trains recorded at Monterey. Each of these swell trains had been analyzed for height and period of the dominant waves. The storm producing each train was identified on the weather maps from the effective origin time and distance derived from the observed frequency-time distribution in the swell in the manner described by Munk, et al. (1963). All were North Pacific storms. The sea-level pressure charts covering the important part of the history of each storm are listed in Table 1, along with the corresponding swell trains recorded at Monterey.

Table I: STORM AND SWELL DATA

A. North Pacific Storms Studied

Storm Designation	Surface Pressure Charts Analyzed (GMT)
1	1200/15 Feb to 1200/17 Feb 67
2	1800/17 Feb to 1800/20 Feb 67
3	1200/12 Nov to 1200/15 Nov 67
4	0000/16 Nov to 0600/19 Nov 67
5	1200/12 Mar to 0600/15 Mar 69

B. Associated Swell Trains Recorded at Monterey

Swell Train Designation	Observed Swell Occurrence at Monterey (GMT)
1	1200/20 Feb to 1600/23 Feb 67
2	0800/23 Feb to 0800 25 Feb 67
3	1200/17 Nov to 2200/20 Nov 67
4	0400/21 Nov to 0600/23 Nov 67
5	2000/18 Mar to 0800/20 Mar 69

2. Determination of Surface Winds

By measuring the spacing between isobars on sea-level pressure charts the average geostrophic wind speed was calculated from:

$$V_g = \frac{K}{2\Omega \rho \sin\theta} \frac{\Delta P}{\Delta n}$$

where V_g = geostrophic wind speed in knots

ΔP = pressure differential in millibars

Δn = isobar spacing in degrees latitude

θ = latitude in degrees

ρ = density of air (1.26×10^{-3} gm/cm^3)

K = units conversion factor (1.725×10^{-6})

Ω = earth's angular speed of rotation (7.29×10^{-5} radians/sec)

In this study, because of the relatively small scale of the weather maps used (1:60,000,000), geostrophic winds were calculated using a 12-millibar interval (3 isobar spacings). Geostrophic winds were converted to surface winds using a surface to geostrophic wind-speed ratio of 0.8. FNWC currently uses an average ratio of 0.78 based on Carstensen's (1967) report showing the variation in the ratio with latitude (Figure 1). In the present investigation, the five storms studied were located between latitudes 31 and 53 degrees North; accordingly, a ratio of 0.8 was considered to be a more representative average for these latitudes. The surface wind direction was assumed to be at a cross-isobar angle of 15 degrees; this agrees with current Fleet Numerical practice.

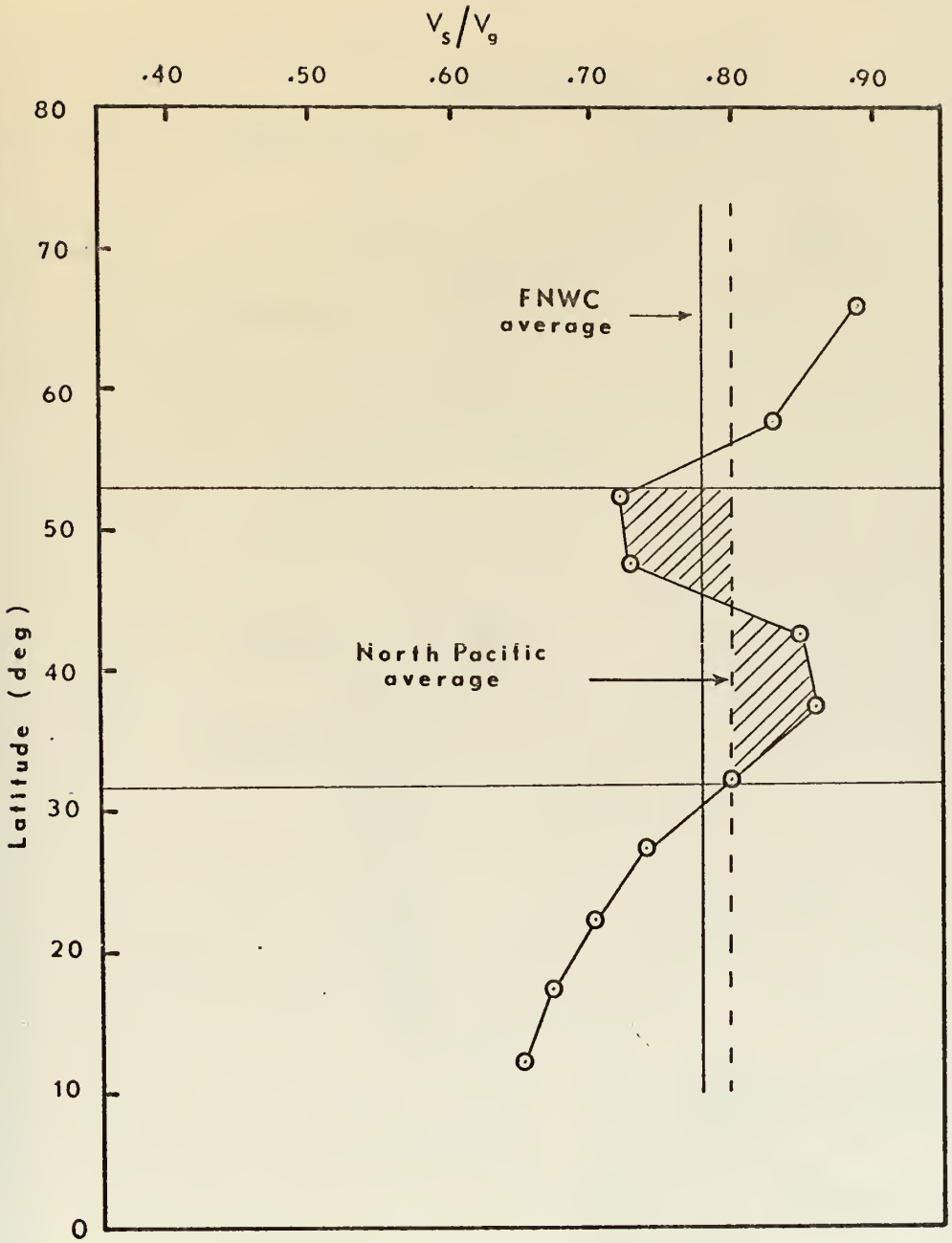

Figure 1: Surface Wind-Geostrophic Wind Ratio (Vs/Vg) as a Function of Latitude (after Carstensen, 1967)

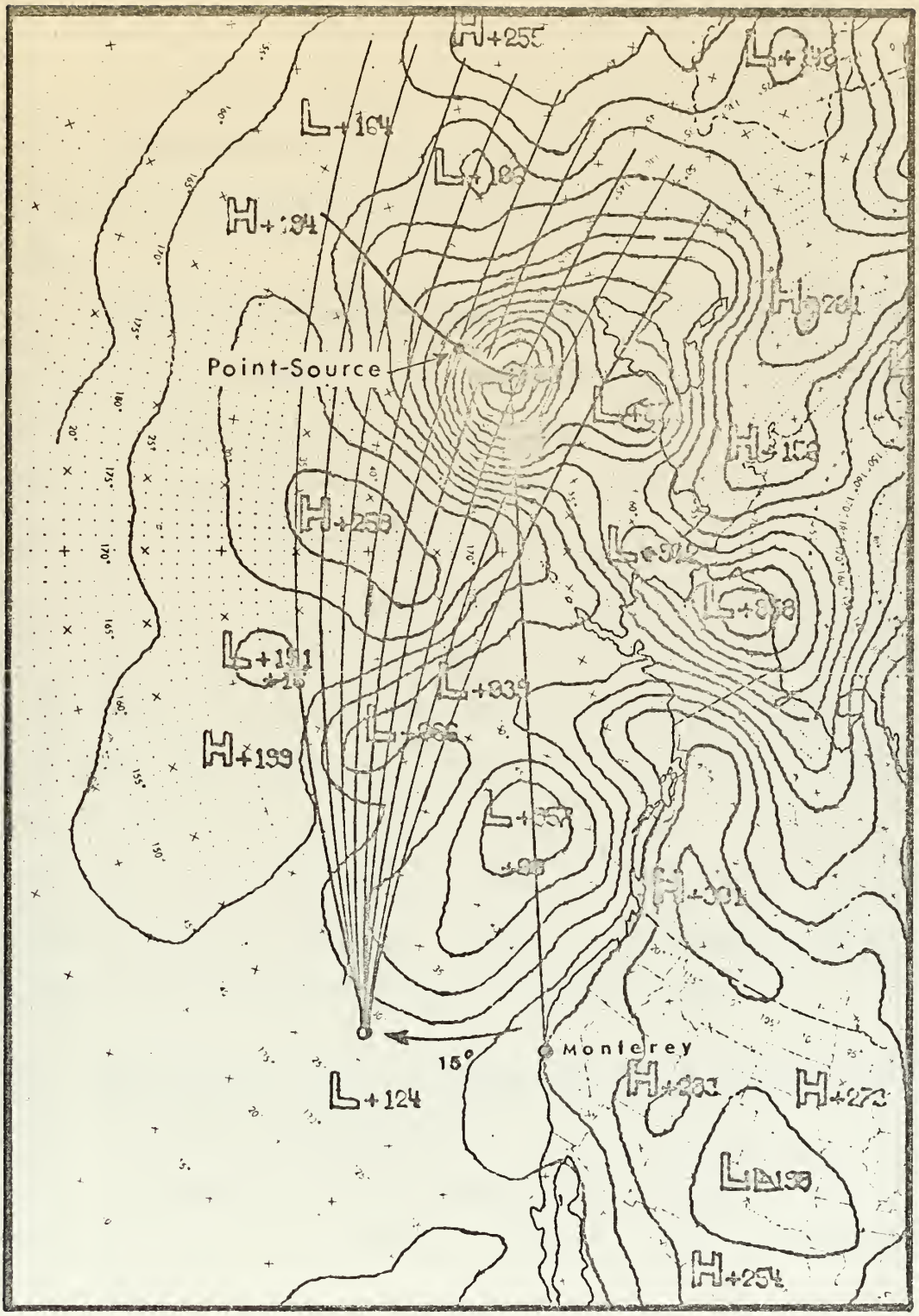

Figure 2: Point-Source Location for Surface Pressure Chart 1200Z/13 Nov 1967

3. Location of the Point-Source

From consideration of the isobar curvature and surface wind-speed profile characteristic of a cyclonic storm, it is assumed that waves of maximum energy propagating toward Monterey must be generated at or close to the point where the maximum surface winds are directed toward Monterey.

In order to identify that location in the cyclonic wind field on a selected weather map, an overlay of great-circle arcs from Monterey was prepared (Figure 2). By rotating the overlay fifteen degrees clockwise about the storm center the locus of points in the storm where the great circle arcs are tangent to the isobars can be determined; this locus represents the storm radius along which are found those surface winds generating waves directly toward Monterey. The point of maximum wind speed along this radius is identified by measuring successive 3 isobar (12-millibar) spacings and locating the midpoint of the strongest pressure gradient. Figure 2 illustrates this technique for a selected surface pressure chart.

4. Specification of the Sea Spectrum at the Point-Source

a. Basic Considerations

Moskowitz (1963) analyzed wave records and corresponding wind measurements taken by ocean weather ships of the United Kingdom in the North Atlantic Ocean and obtained a family of spectra representing fully-arisen sea conditions for certain wind speeds between 20 and 40 knots.

Pierson and Moskowitz (1964) later used the data to test the similarity theory of Kitaigorodskii who proposed that all fully developed seas should have the same non-dimensional spectral form. They showed that within the limit of accuracy of the reported wind speeds, the data of Moskowitz confirmed the theory that a single non-dimensional power spectrum might be used to represent the dimensional spectra for fully arisen seas generated by any wind speed. The non-dimensional spectrum reduced from these data was determined to have its non-dimensional peak value of 2.75×10^{-5} at a non-dimensional frequency of 0.140 using the following non-dimensionalizing conversions:

$$\zeta = f V_s / g \tag{1}$$

$$S(\zeta) = E(f) g^3 / V_s^5 \tag{2}$$

where f = dimensional frequency in hertz

ζ = dimensionless frequency

$E(f)$ = dimensional energy density at frequency f

$S(\zeta)$ = dimensionless energy density at frequency ζ

V_s = surface wind speed in m/sec

g = acceleration of gravity (9.8055 m/sec^2)

Bretschneider (1963) reported that the general analytical formula for a one-dimensional gravity wave spectrum can be written:

$$S(f) = K_2 f^{-m} e^{-(B_2 f^{-n})} \tag{3}$$

where $S(f)$ = spectral energy density for frequency f , and where it can be shown that:

$$B_2 = \frac{m}{n} f_p^n$$

$$K_2 = f_p^m S(f_p) e^{m/n}$$

f_p = frequency of the spectral peak

In a later work, Bretschneider (1963) proposed a spectral form for wind-generated seas based on Equation 3 in which m = 5 and n = 4. Pierson and Moskowitz concluded that for the purpose of forecasting the properties of the larger waves in a wind-generated sea, this spectral form is a good representation.

b. Generation of Energy Spectra

In this investigation, Bretschneider's analytical formula (Equation 3) was used to generate Bretschneider's (1963) spectral form approximation of the Pierson-Moskowitz non-dimensional spectrum over the dimensionless frequency range 0.10 to 0.30, using an IBM 1620 computer. Figure 3 is a plot of this spectrum.

The dimensionless spectrum was used to obtain a dimensional power spectrum at the point-source on each weather chart using the wind speed value calculated for the point-source and the conversion factors of Pierson and Moskowitz (Equations 1 and 2).

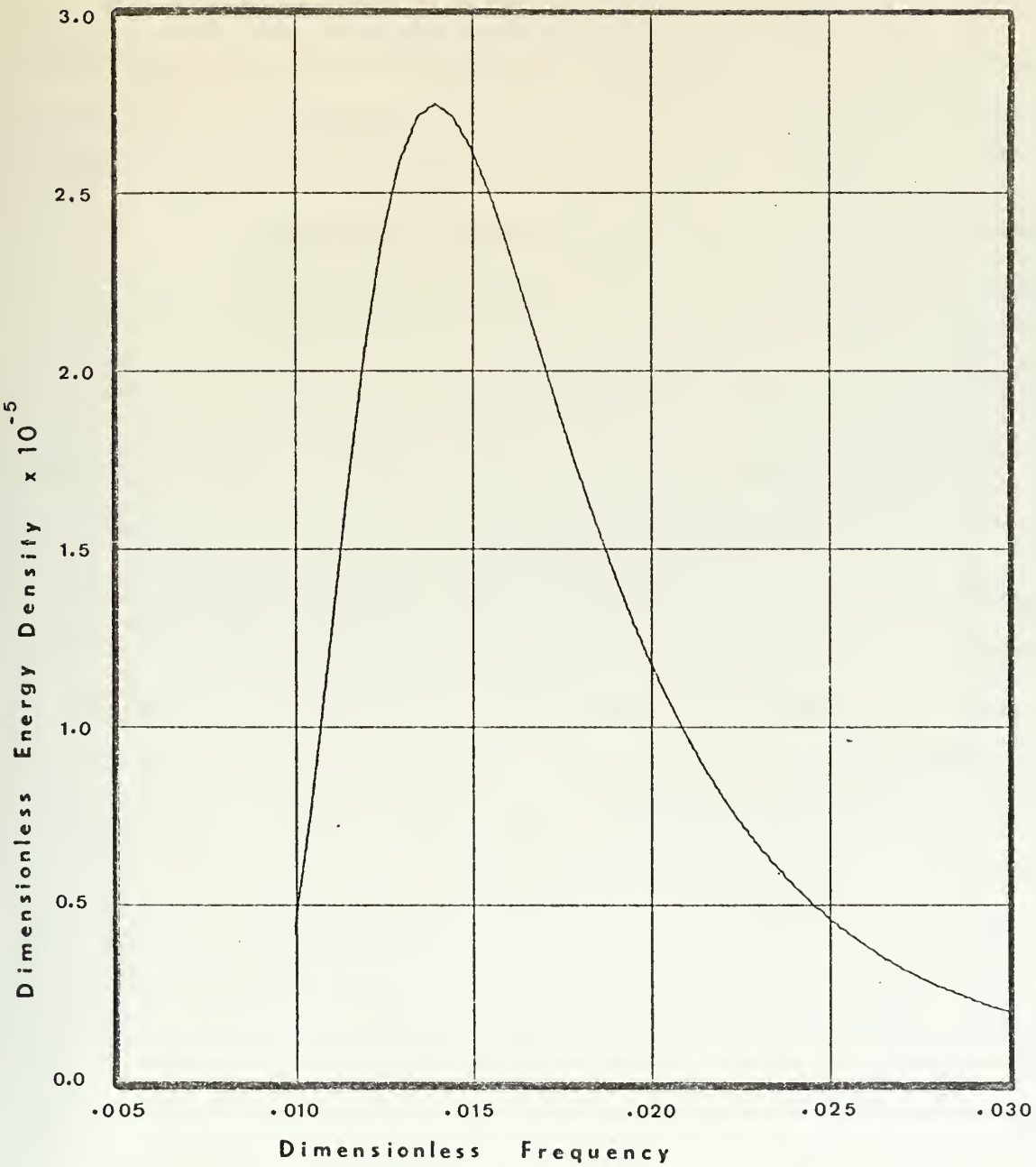

Figure 3: Dimensionless Power Spectrum
(after Bretschneider, 1963)

The spectrum calculated using this procedure represents a fully arisen sea condition. Since the sea at the point-source on most weather maps was clearly not fully arisen, the fully arisen spectrum was truncated at an appropriate cutoff frequency, as proposed by Neumann (1953), to approximate the spectrum of the non-fully developed sea considered to be present. The basis for the procedure devised follows arguments presented by Braunstein (1970).

Braunstein argued that fully arisen seas should be generated when the velocity of the fetch equals the group velocity of the peak swell being generated, since such a coincidence produces an effectively long duration. In the present investigation a group velocity-fetch velocity coincidence was used to effect a duration limit on the fully arisen energy spectrum. If one travels with the dominant waves at their group velocity, the energy put into the sea at a given wind speed is a function of the duration over which the waves remain under the influence of the generating wind field. In the case where the waves travel in the direction of storm movement, as is the circumstance in this study, the longest effective wind duration is achieved for that frequency component whose group velocity equals the speed of movement of the generating source. Lower frequency components, if generated, move faster than the generating source and move ahead of the area of peak winds before they acquire full energy. Higher frequency components require a relatively short wind duration for achieving saturation and remain in that state.

In this study, Neumann's (1953) model of a sharp spectral cutoff was assumed, and the spectrum generated by the peak winds at the point-source on a given weather map was truncated at that frequency having a group velocity equal to the speed of the point-source averaged over the six-hour period just preceding.

This method has some obvious deficiencies. For very large storm speeds, it tends to produce spectra which are more developed than would actually be the case, and for very low-speed storms (including the stationary storm case) the spectra produced are less developed than would be expected. As will be shown, however, for forecasting the characteristics of the dominant swell produced in a moving cyclonic storm, the method produces results which are reasonably consistent with observations.

The problem of specifying the duration associated with the generation of the maximum seas in a moving cyclonic storm of given size, intensity, and speed is not simple and merits additional research.

C. SWELL PROPAGATION

1. Dispersion of Period Components

The spectral components of the predicted seas are then permitted to propagate to Monterey. The arrival time at Monterey from a given point-source is computed for each component using the dispersion relation:

$$t_a = t_o + 4\pi d/g\tau$$

where t_a = arrival time of period component T

t_o = origin time at the point-source (a weather-map time)

d = great circle distance from the point-source to Monterey

T = period in seconds

Figures 4 through 8 are plots of swell period versus time of arrival at Monterey for each of the five storms studied. For each storm there is a set of curves, each of which represents the distribution with time of the components of the wave spectrum arriving at Monterey from a given point-source. Each curve is labeled with a date-time group indicating the map time of the particular sea-level pressure chart containing the point-source from which the curve was derived. The length of each curve is governed by the characteristics of the sea spectrum calculated at the originating point-source. The high frequency end (that component arriving latest in time) is determined by introducing a fixed minimum energy density criterion into the dispersion program; frequencies in the sea spectrum having energy density values less than 1.0 m^2-sec are not plotted. The low frequency end of each curve represents the frequency of spectral cutoff discussed in the previous section.

2. Propagation of Spectral Energy

a. General Considerations

In addition to the effect of dispersion, the energy in the wave spectrum generated at each point-source

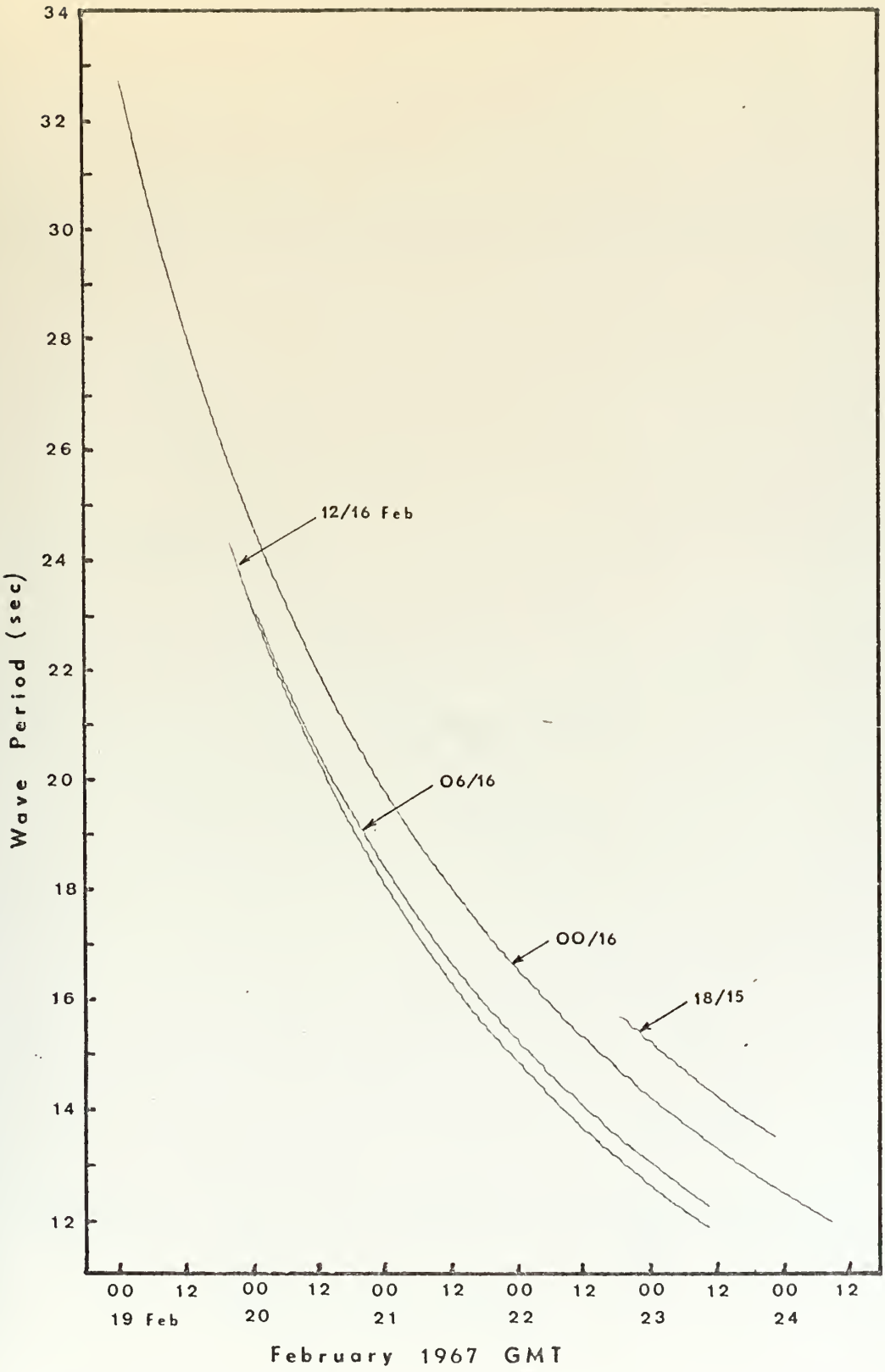

Figure 4: Period-Time Curves for Storm 1

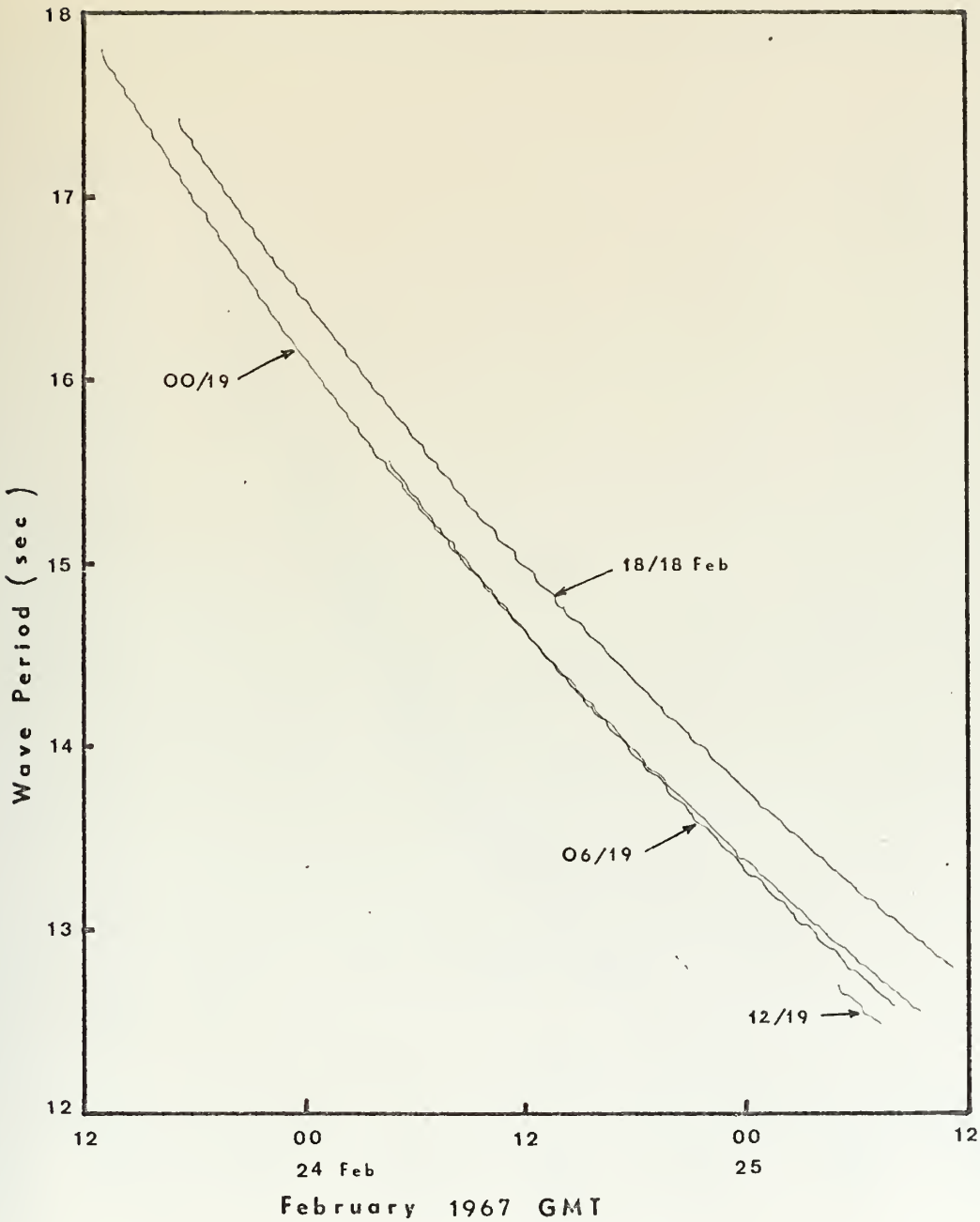

Figure 5: Period-Time Curves for Storm 2

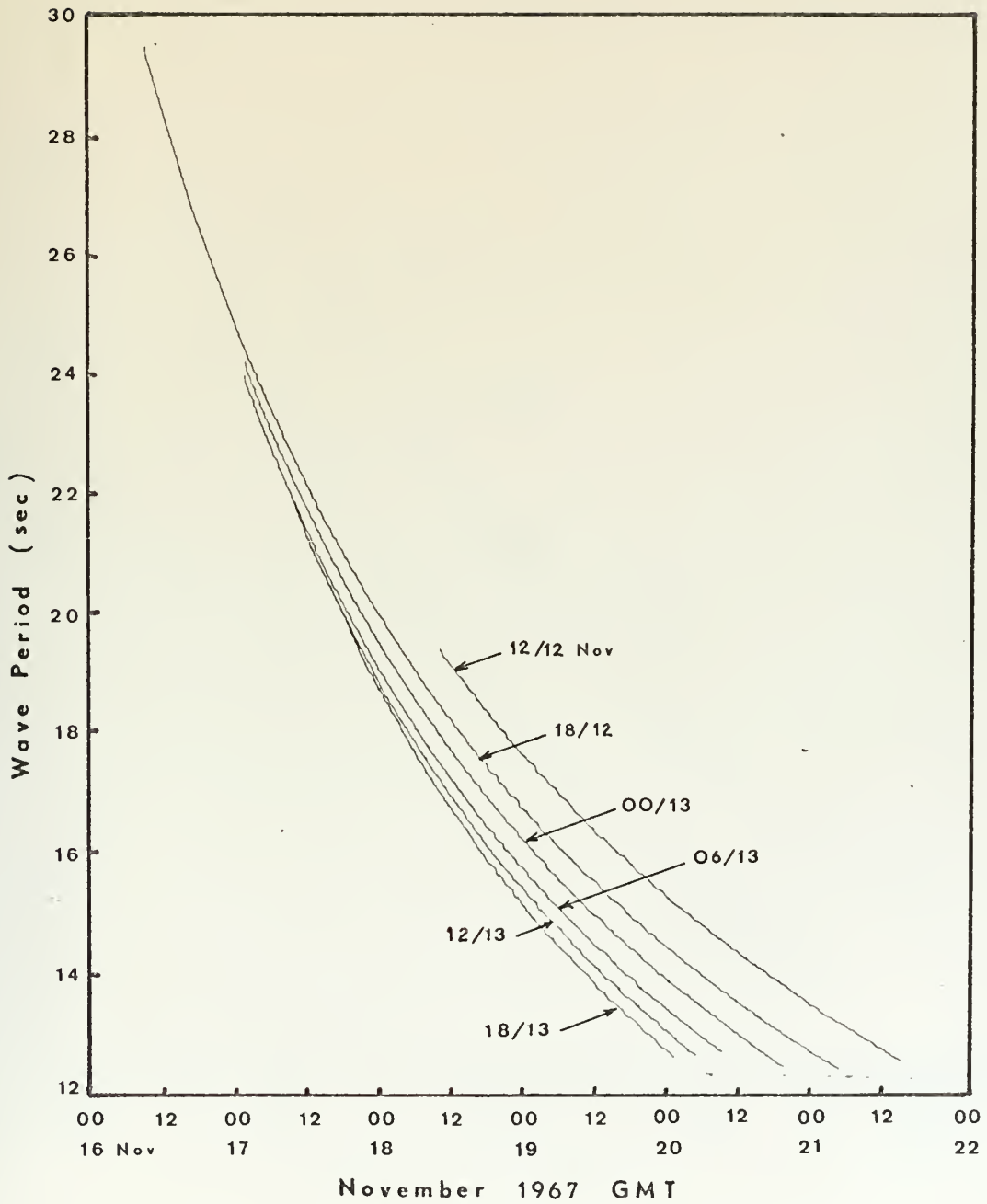

Figure 6: Period-Time Curves for Storm 3

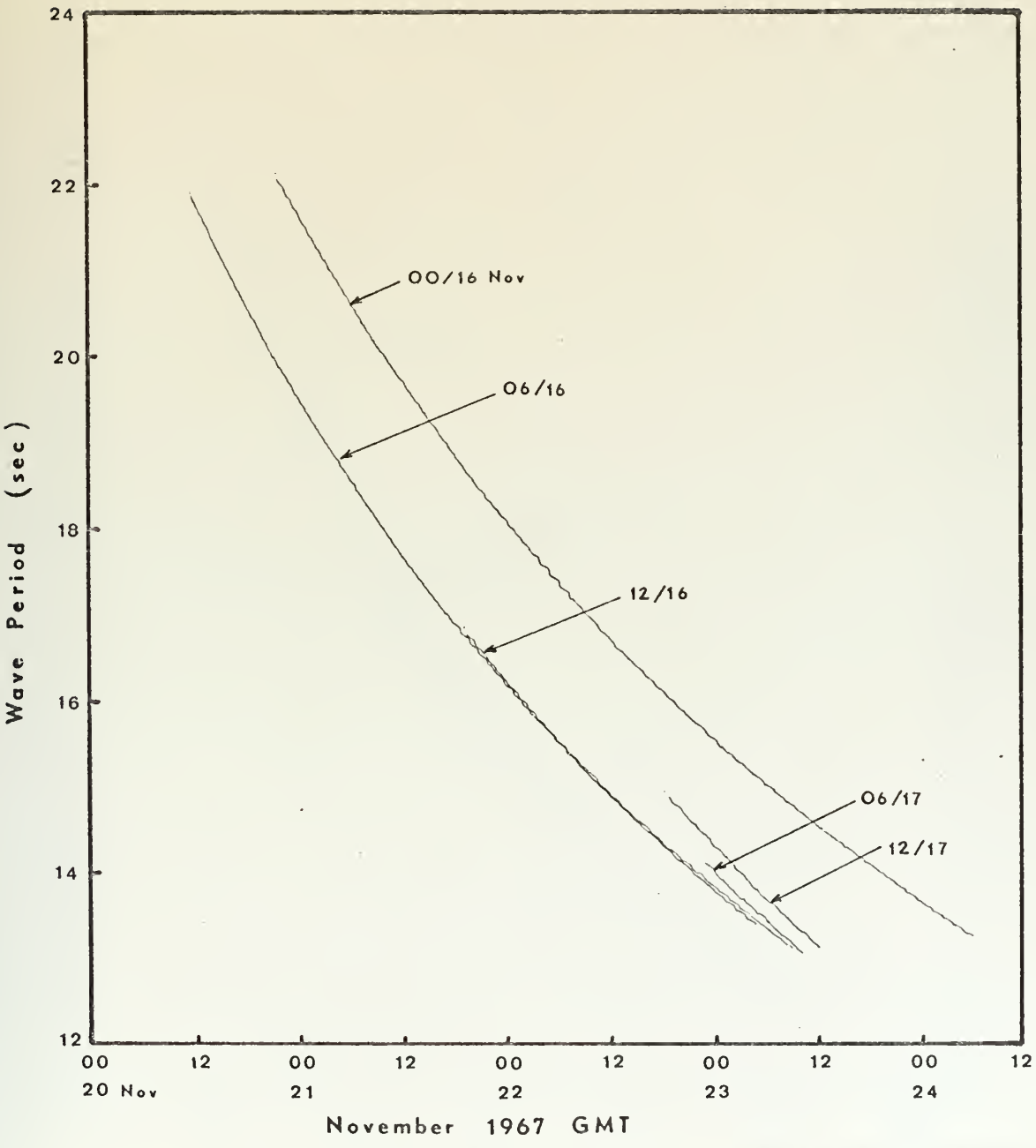

Figure 7: Period-Time Curves for Storm 4

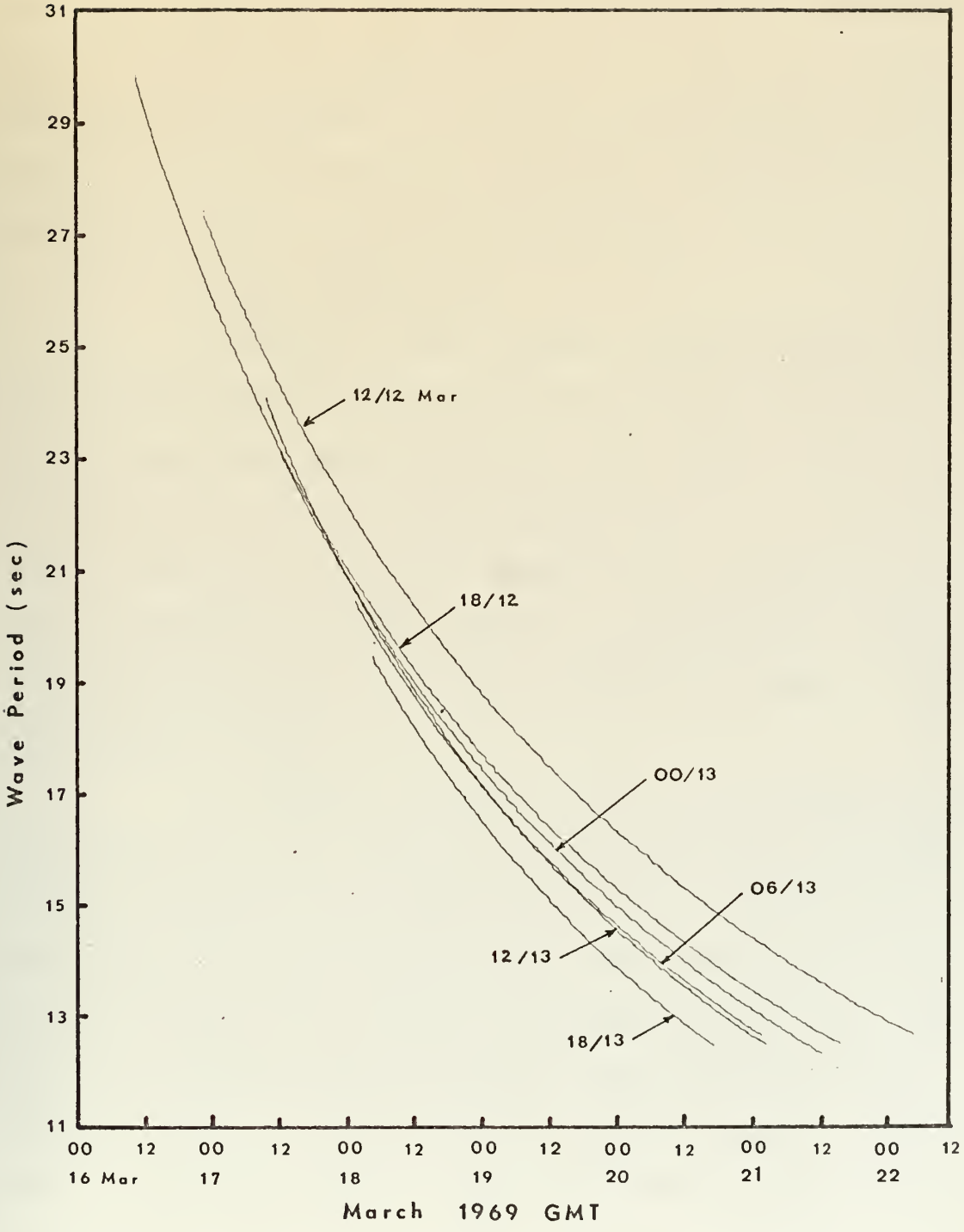

Figure 8: Period-Time Curves for Storm 5

is diminished by the effects of angular spreading and high frequency attenuation during propagation. The angular spreading function is the frequency-independent Neumann function (Figure 9). An attenuation function is used to account for the non-linear processes of wave-wave interaction and wave breaking; it results in dissipation of energy mainly in the high-frequency end of the spectrum with little noticeable effect on the low frequencies.

b. Angular Spreading

Although on each weather map the maximum energy waves being produced are considered to have originated at a point-source, the generating area has a finite width by virtue of the fact that the maximum surface wind speed computed at the point-source is obtained by averaging the wind over a 12-millibar isobar interval. The effective width of the generating area is therefore taken to be equal to this 12-millibar spacing.

An angular spreading factor is calculated using the fetch width, the great circle distance from the point-source to Monterey, and the trigonometric relationships outlined in Pierson, Neumann, and James (1955), as illustrated in Figure 9. Because the surface wind at the point-source is directed toward Monterey, the effective fetch width as viewed from Monterey has a fixed angular relationship to the great circle trajectory from the point-source to Monterey. This circumstance simplifies the geometry of angular spreading and, along with the adoption of a fetch

width defined by the pressure gradient, makes it possible to calculate angular spreading factors as a function of distance and wind velocity.

For practical use, a table of angular spreading factors was computed for wind speeds of 10 to 70 knots, at increments of great circle distance of 60 nautical miles (for distances of 600 to 5000 NM), and at latitude increments of one degree (from 30 to 70 degrees North).

In the present study the swell are propagated spherically along great circle paths; accordingly, the PNJ method, which assumes straight-line propagation, was modified using spherical trignometric relations. A comparison of the calculations using both methods indicated that the slight increase in accuracy obtained using spherical trigonometry was not sufficient for the propagation ranges considered (2500 to 5000 nautical miles) to warrant the more complicated spherical computations.

c. High-Frequency Attenuation

Although the subject of wave-wave interaction and other non-linear processes has received considerable treatment in the recent literature (e.g., Hasselman, (1963), Phillips, (1963), and others), no analytical representation has been derived that is suitable for application to long-range swell prediction. However, Snodgrass, et al. (1966) presented empirical data on the attenuation of selected frequencies observed in their study of long-range propagation of ocean swell in the Pacific. In general, they found

attenuation to be large within the limits of the wind area of the generating storm and negligible beyond the storm. In swell that had travelled a considerable distance from the storm, they also found that below a frequency of 0.06 hertz, attenuation was too small to be measured and above 0.08 hertz, the wave energy was masked by the background level. The empirical attenuation data given by Snodgrass, et al. were logarithmic attenuation coefficients reported in units of decibels per latitude degree of propagation distance. For the range of frequencies 0.06 to 0.08 Hz, these data fit an energy attenuation function of the form:

$$e^{-2\alpha x}$$

where α = modulus of amplitude decay in deg^{-1} = $0.1151\,\beta$

β = logarithmic attenuation coefficient in dB/degree

x = propagation distance in degrees

In this study, the empirical data of Snodgrass, et al. were used, and were extrapolated to provide an estimate of the most likely attenuation at higher frequencies. The extrapolation of the attenuation data is illustrated in Figure 10, a semi-log plot of the logarithmic attenuation coefficient in decibels per latitude degree versus frequency. The empirical data were extrapolated to the frequency at which the logarithmic attenuation function reached a value of 1.0 dB/degree; higher frequencies were assumed to be equally affected by attenuation. Frequencies below 0.06 hertz were similarly assumed to be attenuated by the same amount as the 0.06 hertz component.

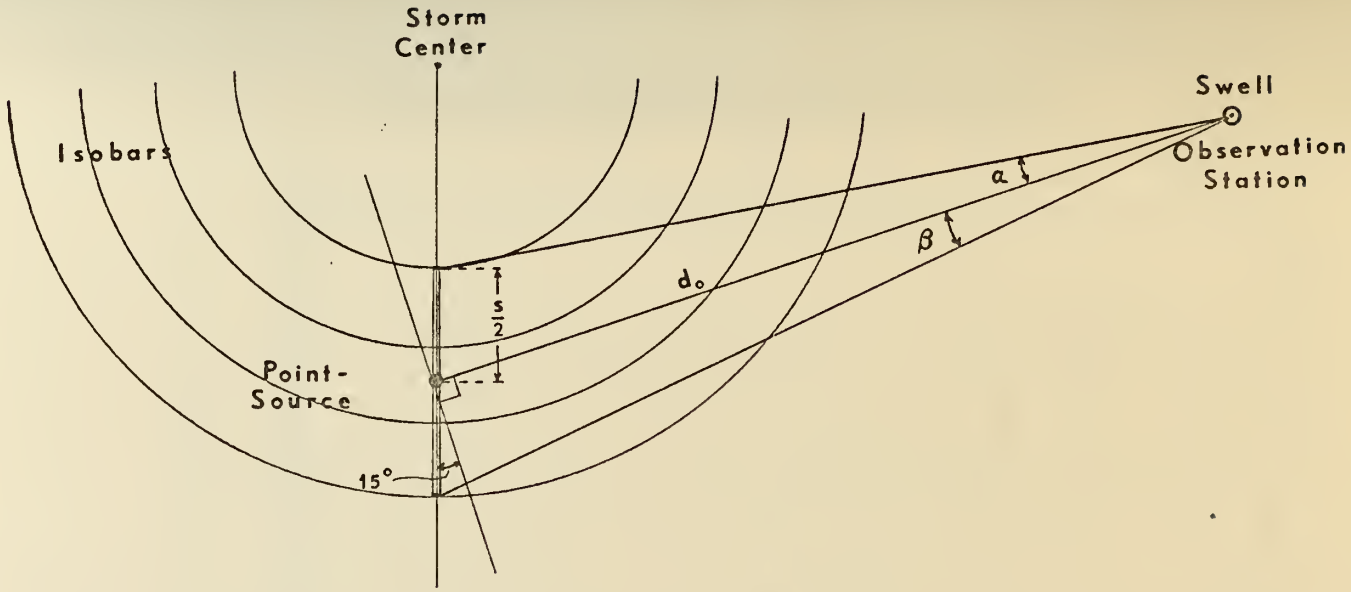

$$F_s\,(\%) = 100\left[\frac{1}{2} + \frac{\Theta}{180^\circ} + \frac{\sin 2\Theta}{2\pi}\right]$$

$$\Theta = \alpha + \beta$$

$$\alpha = \tan^{-1}\left[\frac{\frac{s}{2}\sin 75^\circ}{d_o + \frac{s}{2}\sin 15^\circ}\right]$$

$$\beta = \tan^{-1}\left[\frac{\frac{s}{2}\sin 75^\circ}{d_o - \frac{s}{2}\sin 15^\circ}\right]$$

d_o = great circle distance from point-source to observation station

s = 12 millibar spacing

F_s = angular spreading factor

Figure 9: Calculation of the Angular Spreading Factor, F_s

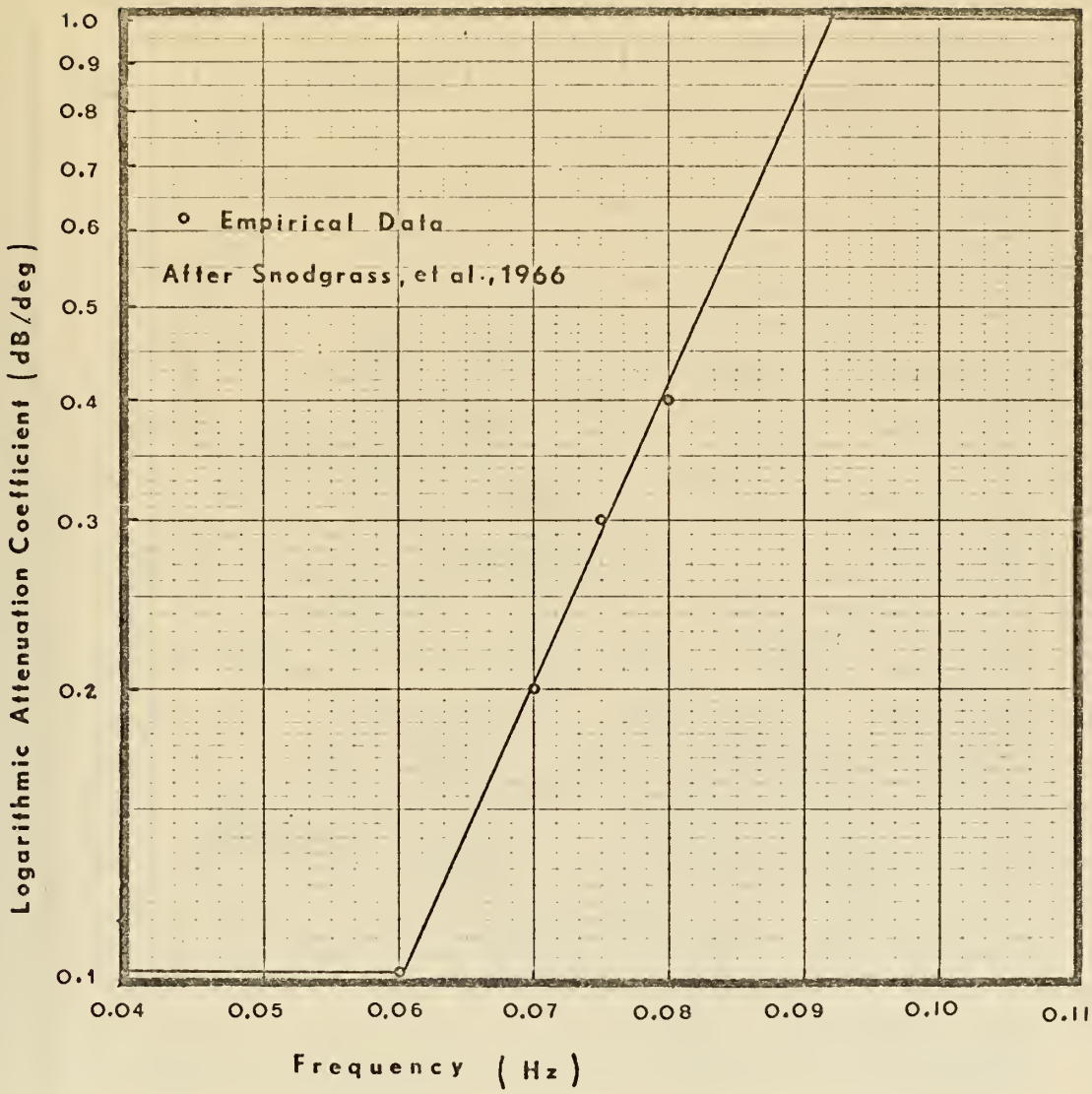

Figure 10: High Frequency Attenuation Function

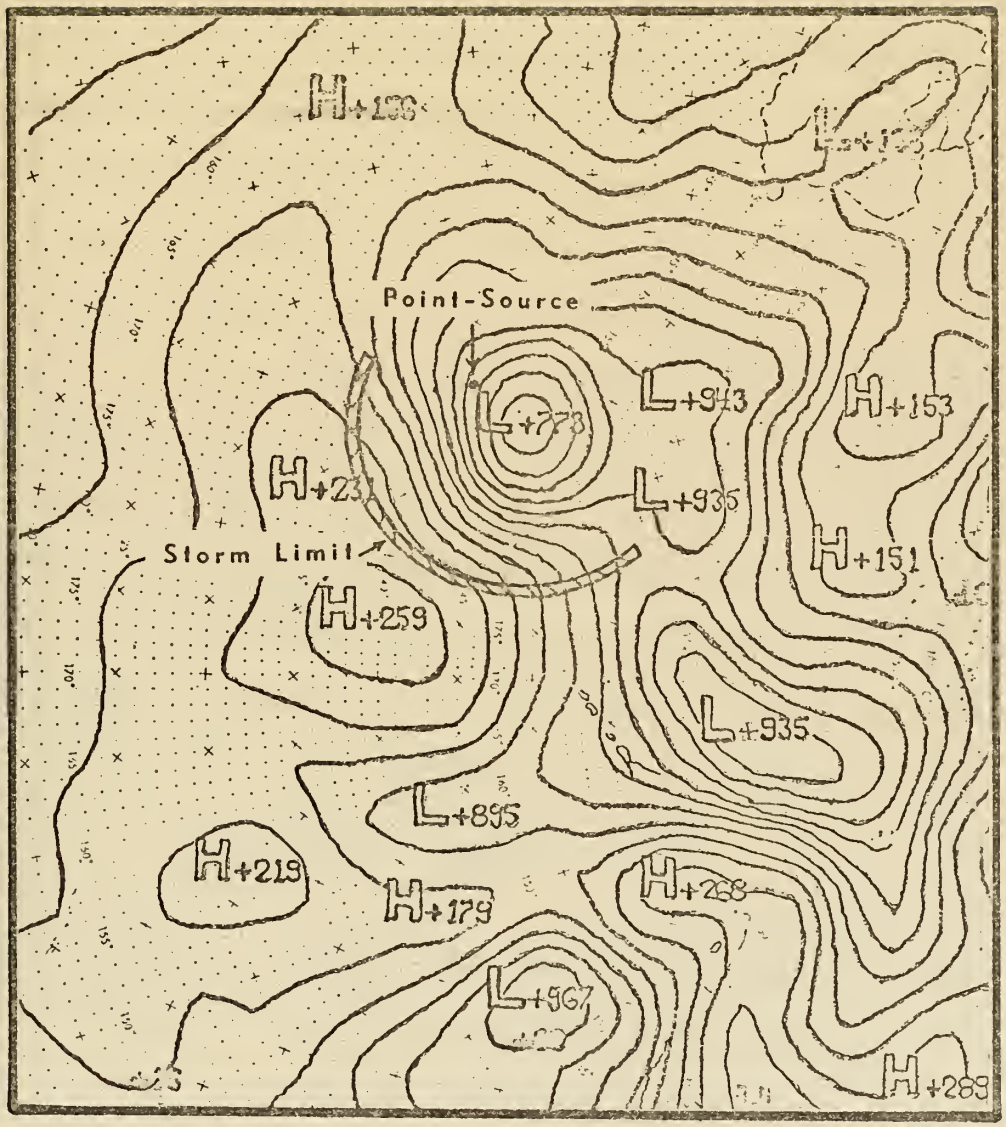

Figure 11: Storm Limit for Surface Pressure Chart 0000Z/13 Nov 1967

Following the observation of Snodgrass, et al. that attenuation beyond the area encompassing the storm fetch was negligible, the energy attenuation function of Snodgrass, et al. (1966) was applied over the propagation distance from the point-source to the outer limit of the storm. The storm limit was taken to be the boundary beyond which the isobars no longer follow the circular pattern of the storm and thus can no longer be associated with the counter-clockwise flow around the low-pressure system. Figure 11 shows the location of the storm limit on a selected sea-level pressure chart.

d. Propagation of Spectral Energy

The energy dissipating effects of angular spreading and attenuation during propagation of the swell from the point-source on each successive weather chart to Monterey is accounted for by applying the spreading and attenuation factors to the energy-density values of selected periods covering the entire spectrum. For a given frequency component, f_i, energy density propagation loss is computed by:

$$\left[A_o(f_i)\right]^2 = \left[A(f_i)\right]^2 F_s\, e^{-2\alpha x}$$

where $\left[A_o(f_i)\right]$ = energy density in deep water at Monterey

$\left[A(f_i)\right]$ = energy density at point-source

F_s = angular spreading factor

$e^{-2\alpha x}$ = attenuation function

By propagating each of these dissipated energy-density values to Monterey at the appropriate group velocity, the distribution of spectral energy with arrival time is obtained

for each point-source. This energy density-time curve is referred to here as a "propagated spectrum". Plots of the propagated spectra computed for deep water off Monterey for the five storms studied are shown in Figures 12 through 16.

In each figure the uppermost envelope that can be drawn to the family of spectra shown is considered to represent the total propagated spectrum for the actual swell train that would be expected off Monterey. It may be seen in the case of Storm 1 (Figure 12), that the spectrum generated at the time of the weather chart of 0000Z/16 February 1967 had sufficient energy in all frequencies to dominate the other spectra arriving off Monterey. For the other storms, it is seen that the swell at Monterey is dominated at different times by waves arriving from different locations along the storm path.

The frequency associated with a particular energy density in a selected propagated spectrum cannot be read from Figures 12 through 16, but may be determined from the corresponding period-time curve (Figures 4 through 8). All spectra shown in Figures 12 through 16 are greatly reduced in energy in the high frequencies relative to the low frequencies compared to the spectra present at the source-points. The truncated propagated spectra that may be seen in the figures are non-fully arisen spectra.

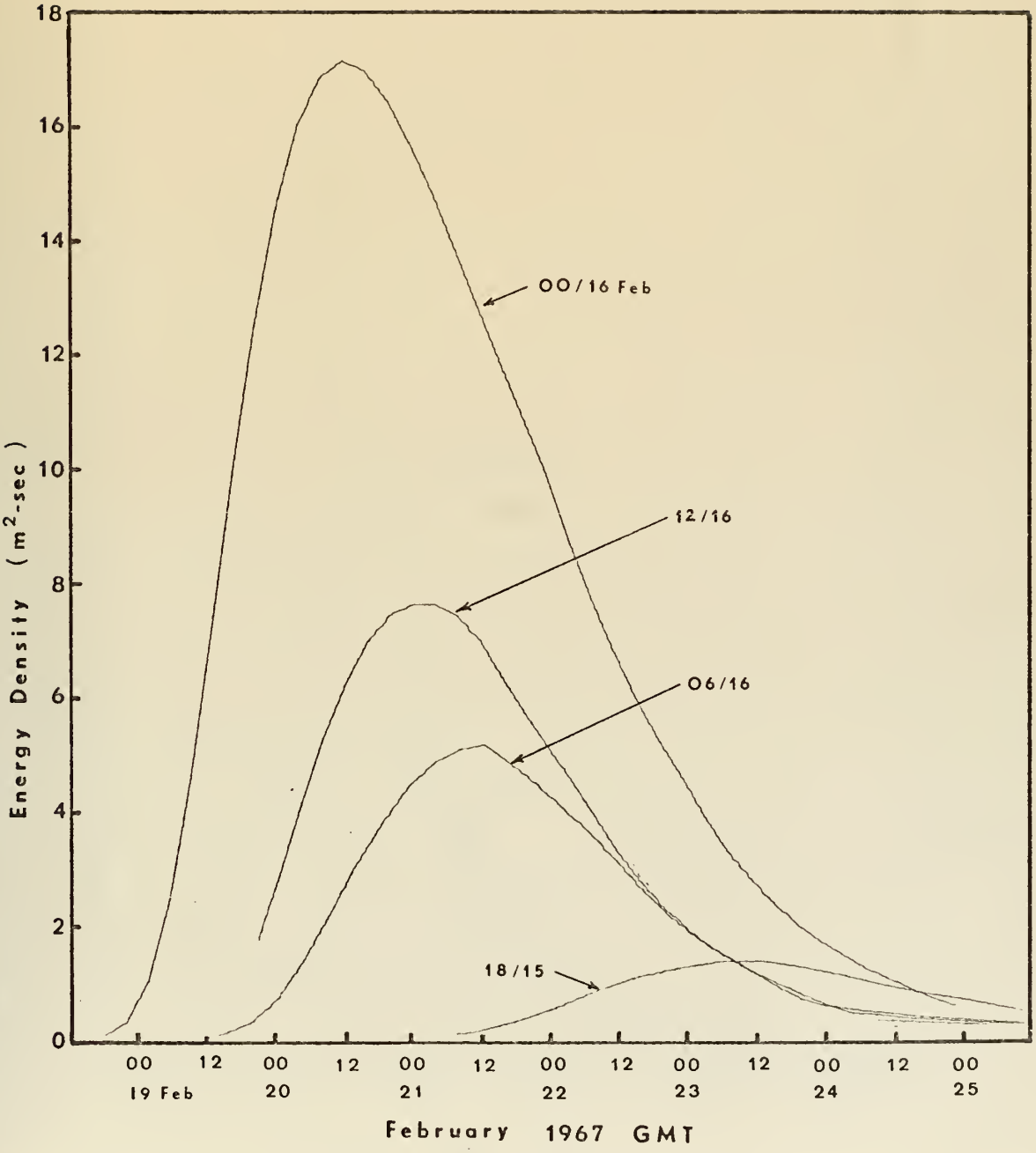

Figure 12: Propagated Spectra for Storm 1

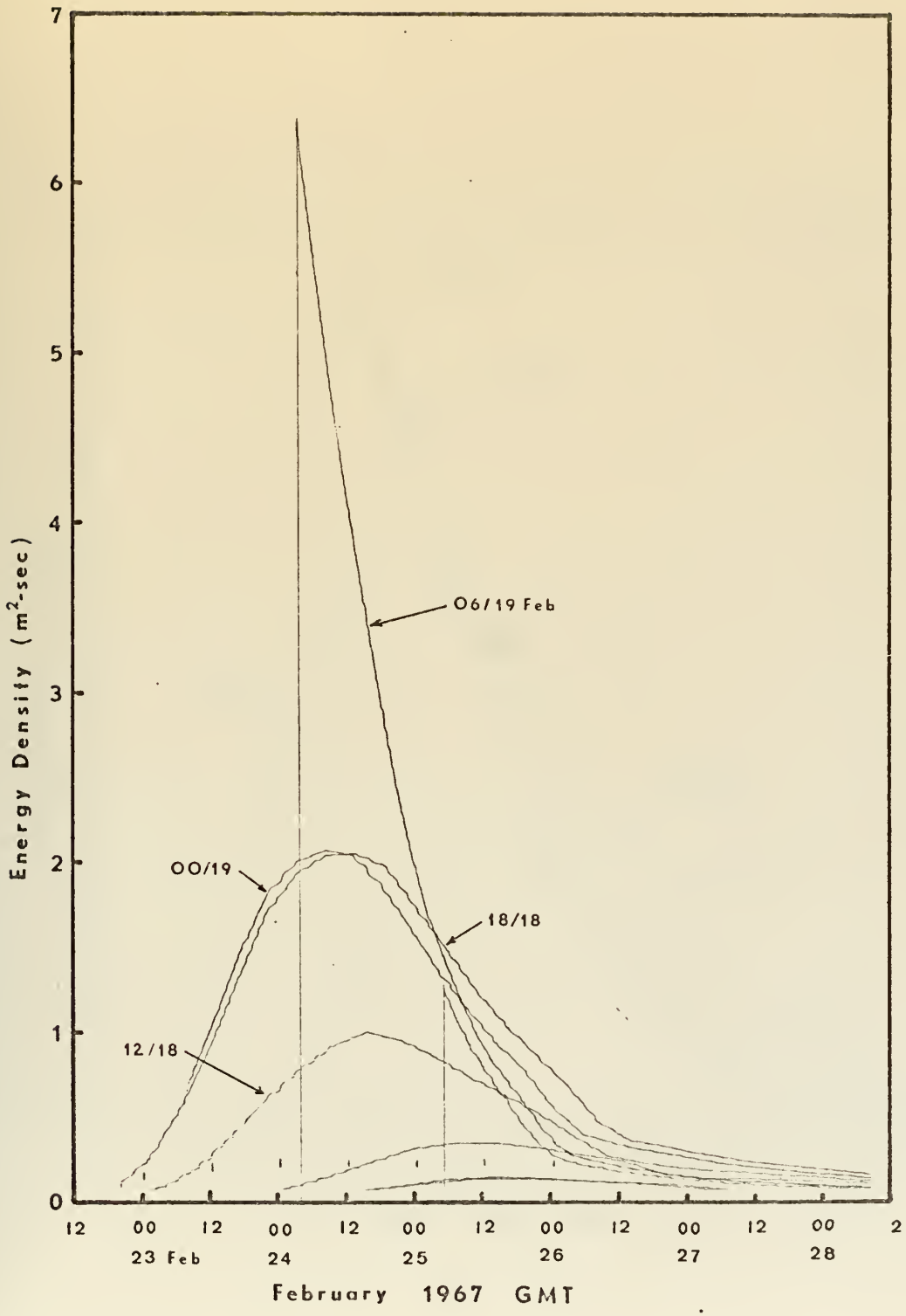

Figure 13: Propagated Spectra for Storm 2

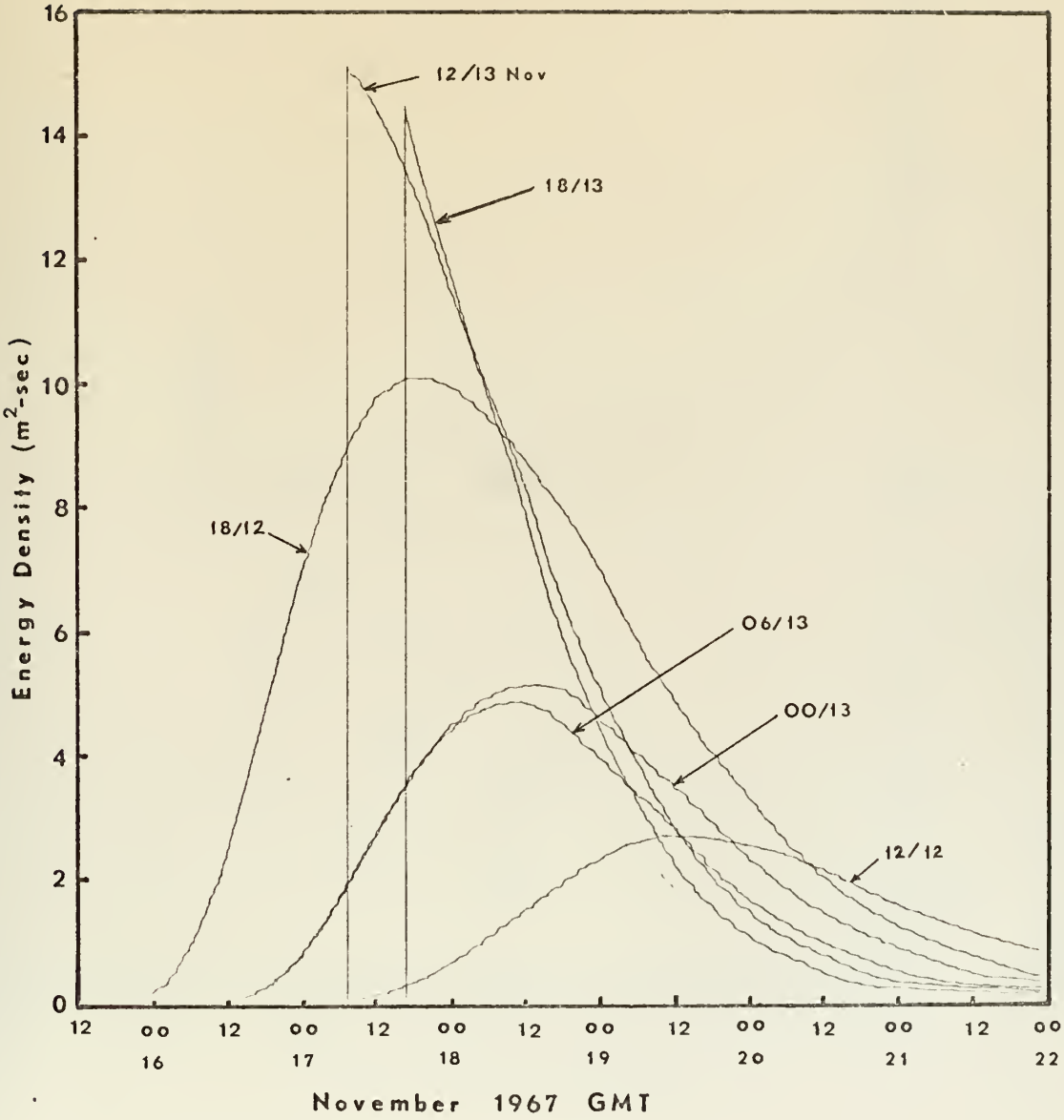

Figure 14: Propagated Spectra for Storm 3

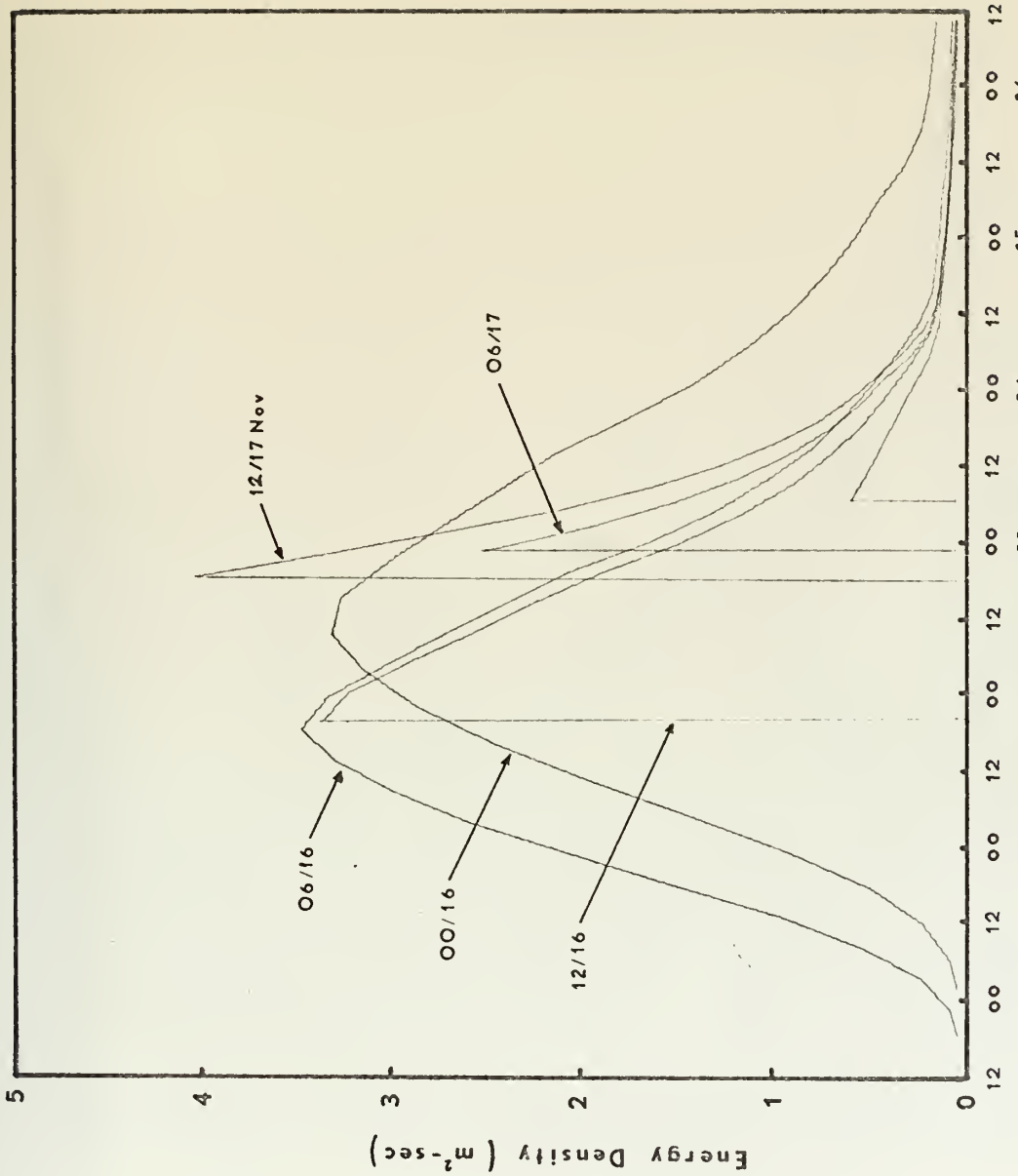

Figure 15: Propagated Spectra for Storm 4

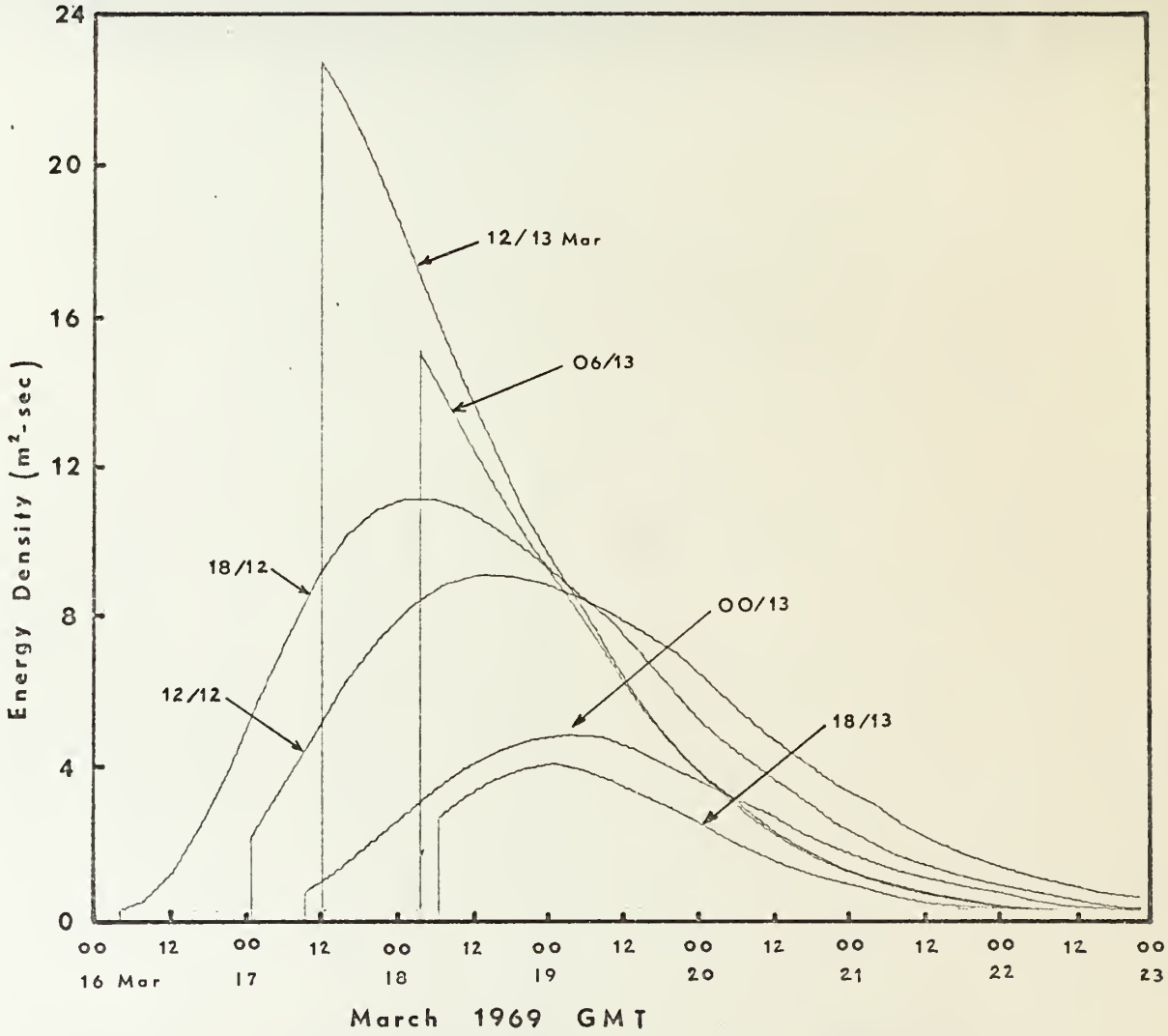

Figure 16: Propagated Spectra for Storm 5

D. PREDICTION OF SWELL CHARACTERISTICS

1. Deep Water Period Prediction

Each curve in Figures 4 through 8 potentially represents the period-time variation of the dominant energy swell arriving at Monterey from one of the five storms. The particular curve or portion thereof containing the dominant energy at a given moment can be determined by referring to Figures 12 through 16. The upper envelope of the family of propagated spectra shown in each figure represents the time distribution of the dominant energy waves in the combined swell arriving from all point-sources. The date-time group identifying each spectrum refers to the map time of the point-source from which the spectrum was derived, and can be used to relate the spectrum to a particular period-time curve (in Figures 4 through 8).

The portions of those period-time curves containing the dominant energy were identified in this way and appear in Figures 17 through 21 as heavy lines. The dots plotted in each figure represent observed period data and are discussed in a later section.

The reader should note that the heavy lines in Figures 17 through 21 represent the predicted distribution with time of the dominant swell periods in deep water at the sensor site. The effects of shoal-water modifications to the arriving swell are discussed later.

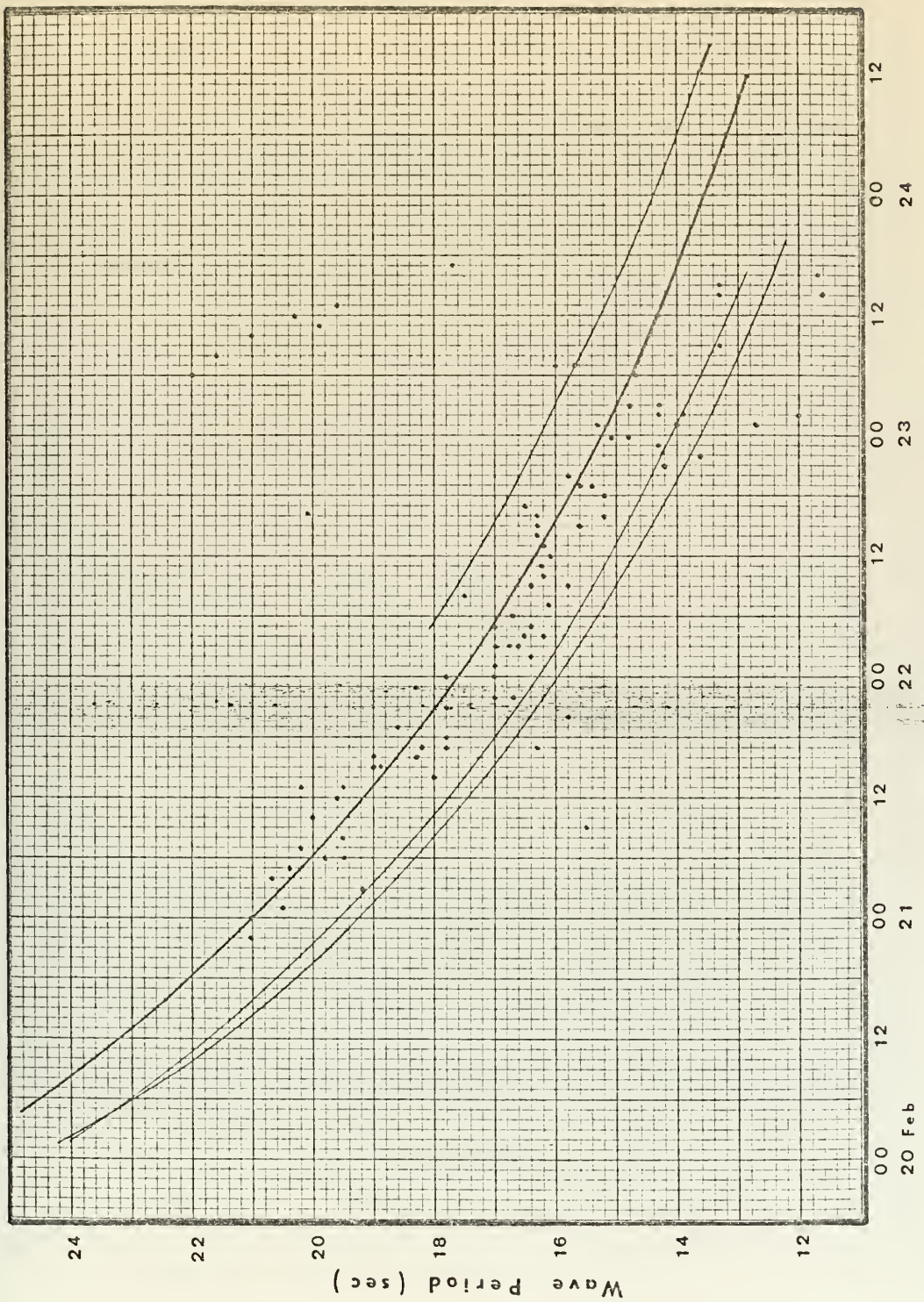

Figure 17: Observed and Predicted Periods for Storm 1

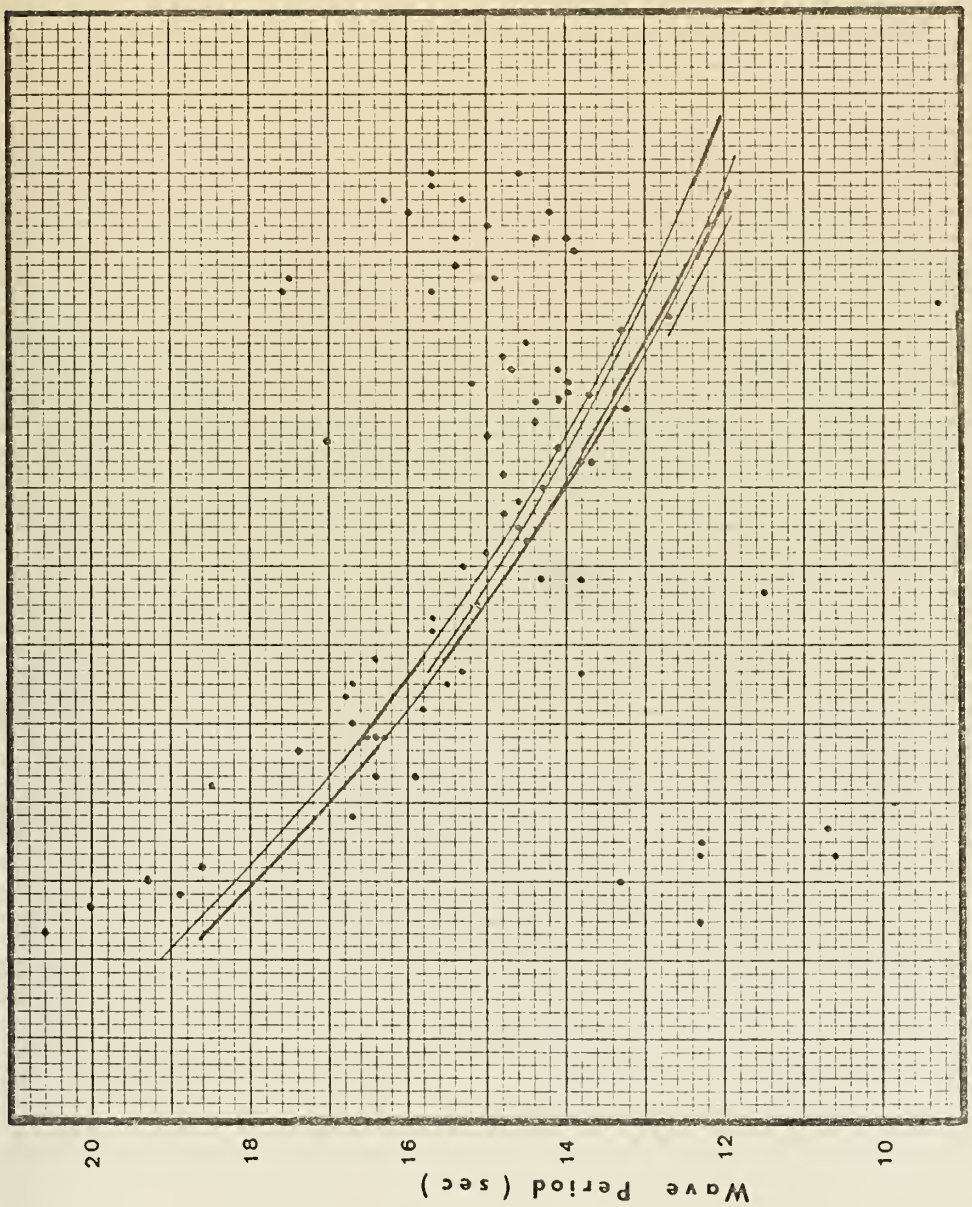

Figure 18: Observed and Predicted Periods for Storm 2

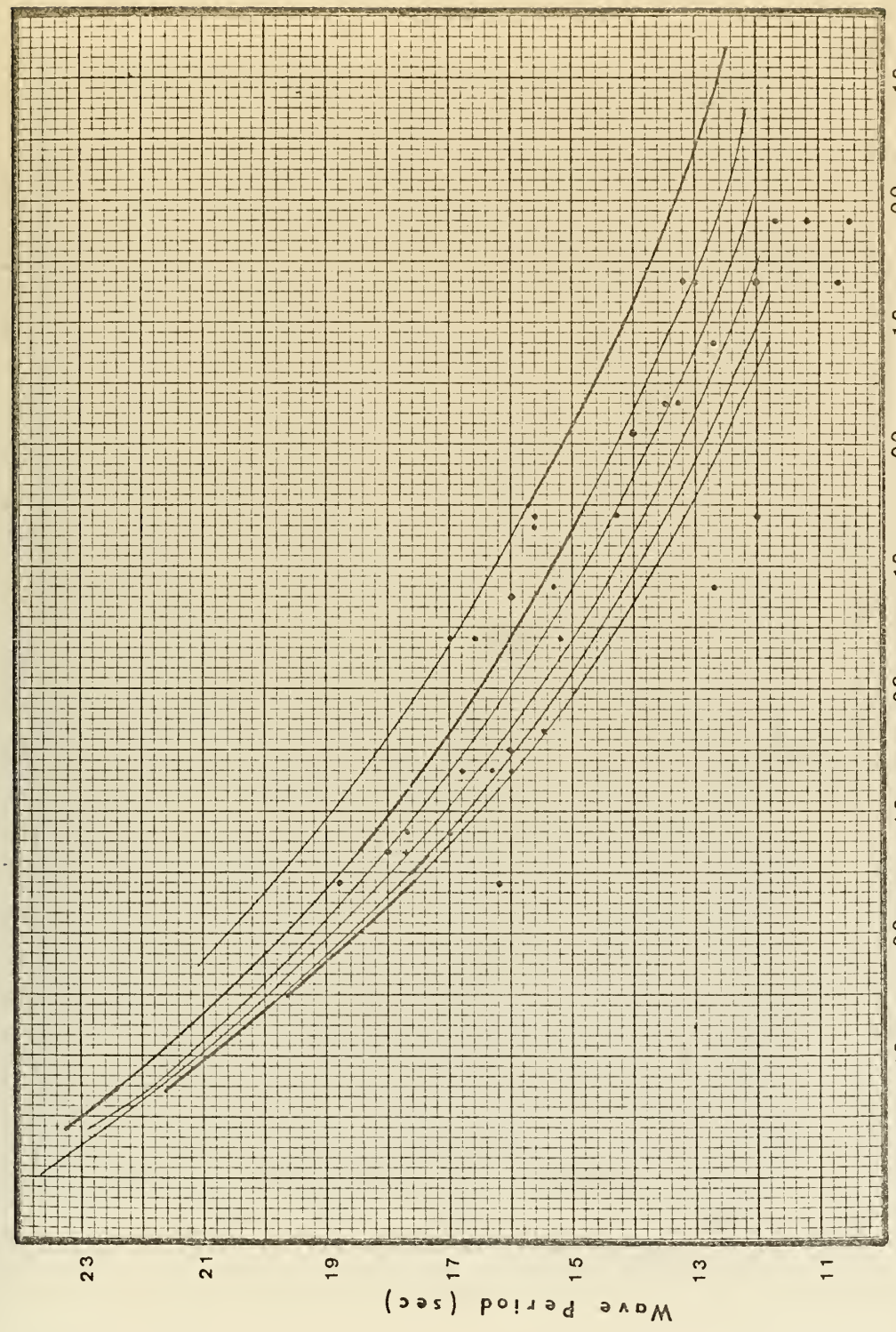

Figure 19: Observed and Predicted Periods for Storm 3

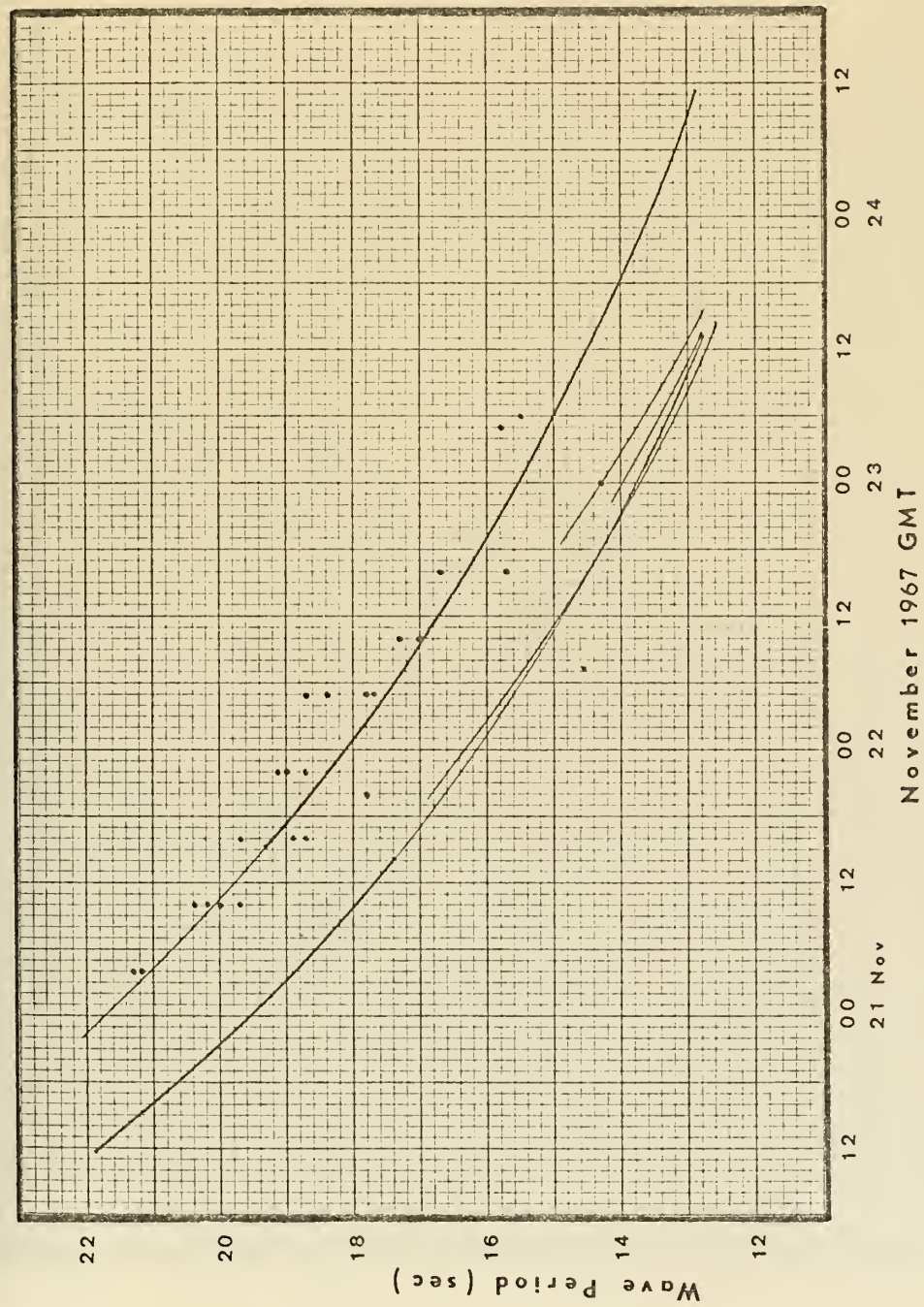

Figure 20: Observed and Predicted Periods for Storm 4

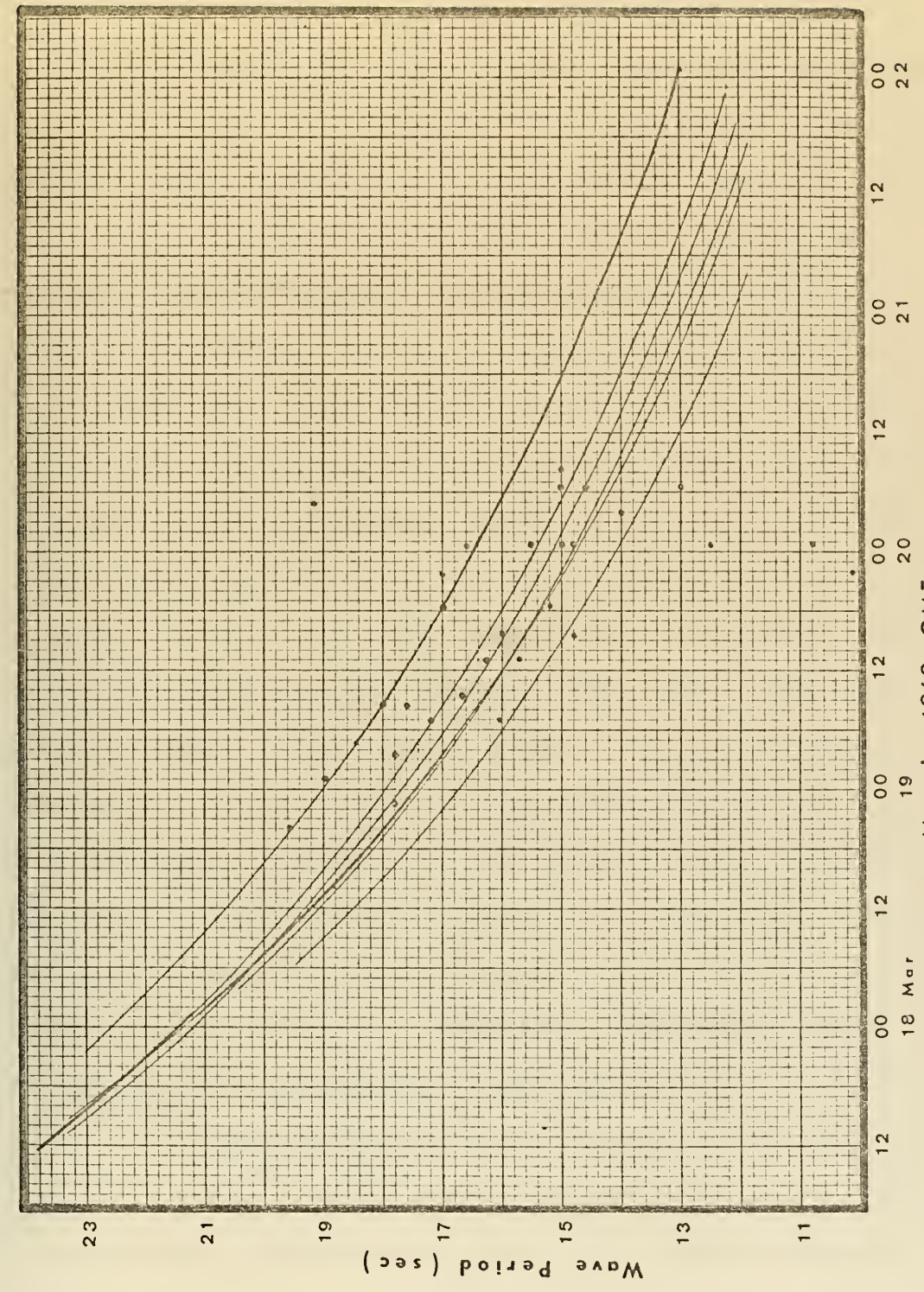

Figure 21: Observed and Predicted Periods for Storm 5

2. Deep Water Height Prediction

a. Estimation of Arriving Swell Energy

A moving storm may be viewed as the source of an infinite number of energy spectra generated during the storm's lifetime. The family of energy-time curves for Monterey shown in Figures 12 through 16, then, are derived from a finite number of selected spectra; specifically, one spectrum associated with each weather map at the point-source identified. By making a time-cut through one of these composites, the energy densities of the spectral components arriving at Monterey at that particular time can be read from the propagated spectra. The period of the waves associated with each of these energy-densities can be read from the corresponding period-time curve (Figures 4 through 8) by making an identical time-cut. Thus, for any selected time, a plot can be made of energy density versus frequency. A continuous spectrum drawn through the points of such a plot represents the predicted energy spectrum of the swell in deep water at Monterey at that time. Figure 22 illustrates these predicted spectra for a series of arrival times for Swell Train 3. The area under each spectrum is proportional to the predicted energy in the arriving swell.

b. Calculation of Swell Heights from Energy Estimates

The total energy in a sea is found by integrating the energy spectrum over the full range of frequencies from 0 to ∞. This energy value, if the approximate spectral form is known, can also be related to the statistical distribution of wave heights in the sea. Longuet-Higgins

(1952) has shown that for narrow band spectra (i.e., swell) the significant wave height, the average of the highest third of the waves in a wave record, is given by:

$$H_{1/3} = 2.83\sqrt{E} \qquad (4)$$

where $H_{1/3}$ = significant wave height

E = total energy in the spectrum

If the predicted swell spectra are sufficiently narrow banded in the sense implied by Longuet-Higgins (1952), this statistical relationship provides a means for computing the swell height distribution with time from the predicted energy-time distribution.

3. Refraction and Shoaling Modifications

a. Shoal Water Height Prediction

The wave sensor used to obtain the observed swell height at Monterey for the five storms studied was located in shoal water; accordingly, the effects of refraction and shoaling had to be considered in order to compare observed heights with heights derived from the computed swell energy.

Since refraction effects are dependent on the direction of swell arrival, and directional information was not recorded, two procedural alternatives presented themselves: the arrival direction of the observed swell could be estimated, and the observed heights adjusted to remove the effects of refraction and shoaling; or the predicted heights could be modified for these effects and compared

with the shoal water data as observed at the sensor site. The latter course of action was chosen because an arrival azimuth for the swell train propagated from each point-source is a function of the great circle path between the point-source and Monterey.

To illustrate the procedure used to calculate the height distribution in the swell at the wave-gage site, Storm 3 will be used as an example (Figure 22). The individual energy-density values determined from the deep water spectral time-cuts, indicated by the dots in the figure, are modified for the effects of refraction and shoaling using the relation:

$$\left[A_s(f_i)\right]^2 = \left[A_o(f_i)\right]^2 \cdot K_r \cdot K_s \qquad (5)$$

where $\left[A_s(f_i)\right]^2$ = shoal-water energy density associated with frequency f_i

$\left[A_o(f_i)\right]^2$ = deep-water energy density

K_r = refraction coefficient

K_s = shoaling coefficient (water depth 30 feet)

Refraction coefficients for the sensor site are shown in Figure 23; the data were compiled for the sensor site from a number of manually drawn refraction diagrams prepared as a laboratory exercise by former students at the Naval Postgraduate School.

The energy in the swell arriving at the sensor site at a selected time is then approximated using the modified energy density values in the step-wise integration scheme:

$$E_s(t) = \sum_{i=1}^{n-1} \left\{ \left[A_s(f_i) \right]^2 + \left[A_s(f_{i+1}) \right]^2 \right\} \frac{\Delta f}{2} \qquad (6)$$

where $E_s(t)$ = total shoal-water energy in swell arriving at time t

$\left[A_s(f_i) \right]^2$ = modified energy-density value associated with frequency f_i

n = number of energy-density values used in the approximation

Δf = frequency band between f_i and f_{i+1}

Figure 24 illustrates the shoal water energy spectra for Swell Train 3 at selected times.

Predicted values of significant swell height in shoal water may then be computed from these shoal-water energy computations using Equation 4. Predictions of significant wave height for the swell arriving at the wave gage site from Storm 3 are shown in Figure 26.

b. Shoal Water Period Prediction

As a result of refraction and shoaling, the energy density associated with a given period may be expected to differ at a shoal water site from the deep water value. Because these processes are frequency dependent, a shift of the dominant energy may occur from one period-time curve to another as the swell passes from deep to shoal water.

A prediction of the dominant periods in shoal water is obtained by plotting the periods of maximum energy density in the shoal water spectra as a function of arrival

time. Figure 28 illustrates the predicted shoal water period-time curve for Swell Train 3, as determined from the shoal water energy spectra shown in Figure 24.

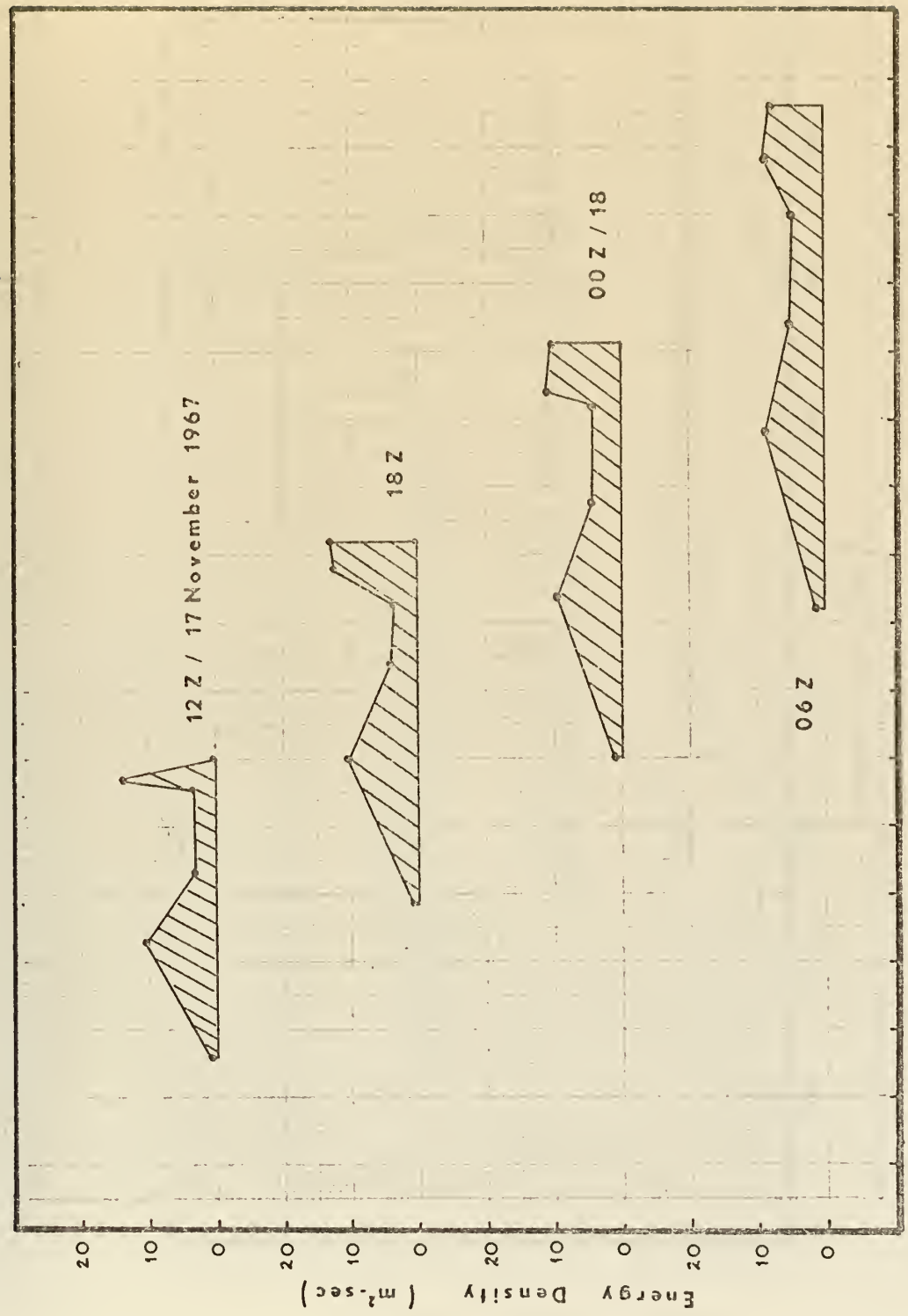

Figure 22: Predicted Deep Water Swell Energy Spectra for Swell Train 3

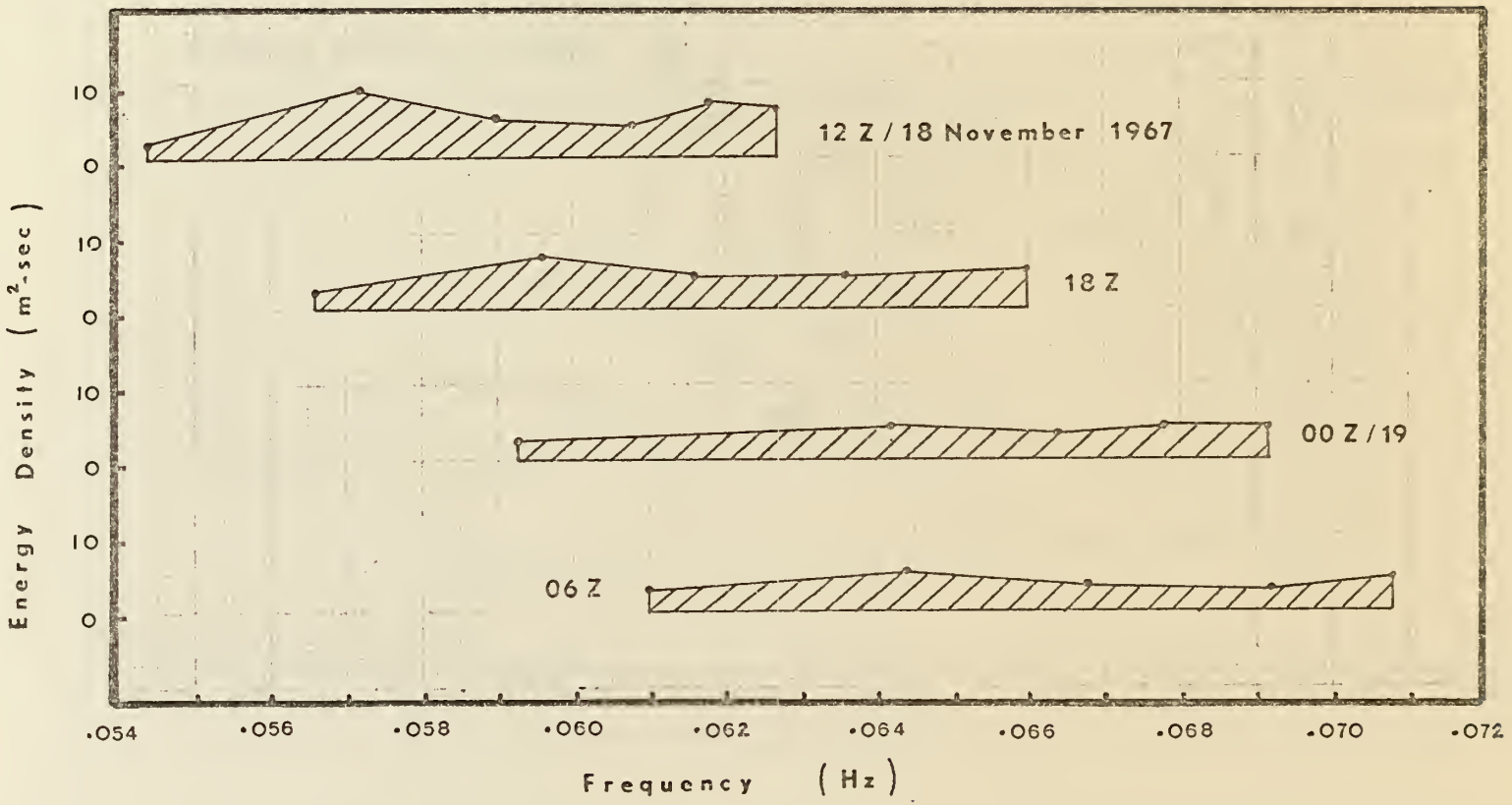

Figure 22: (Continued)

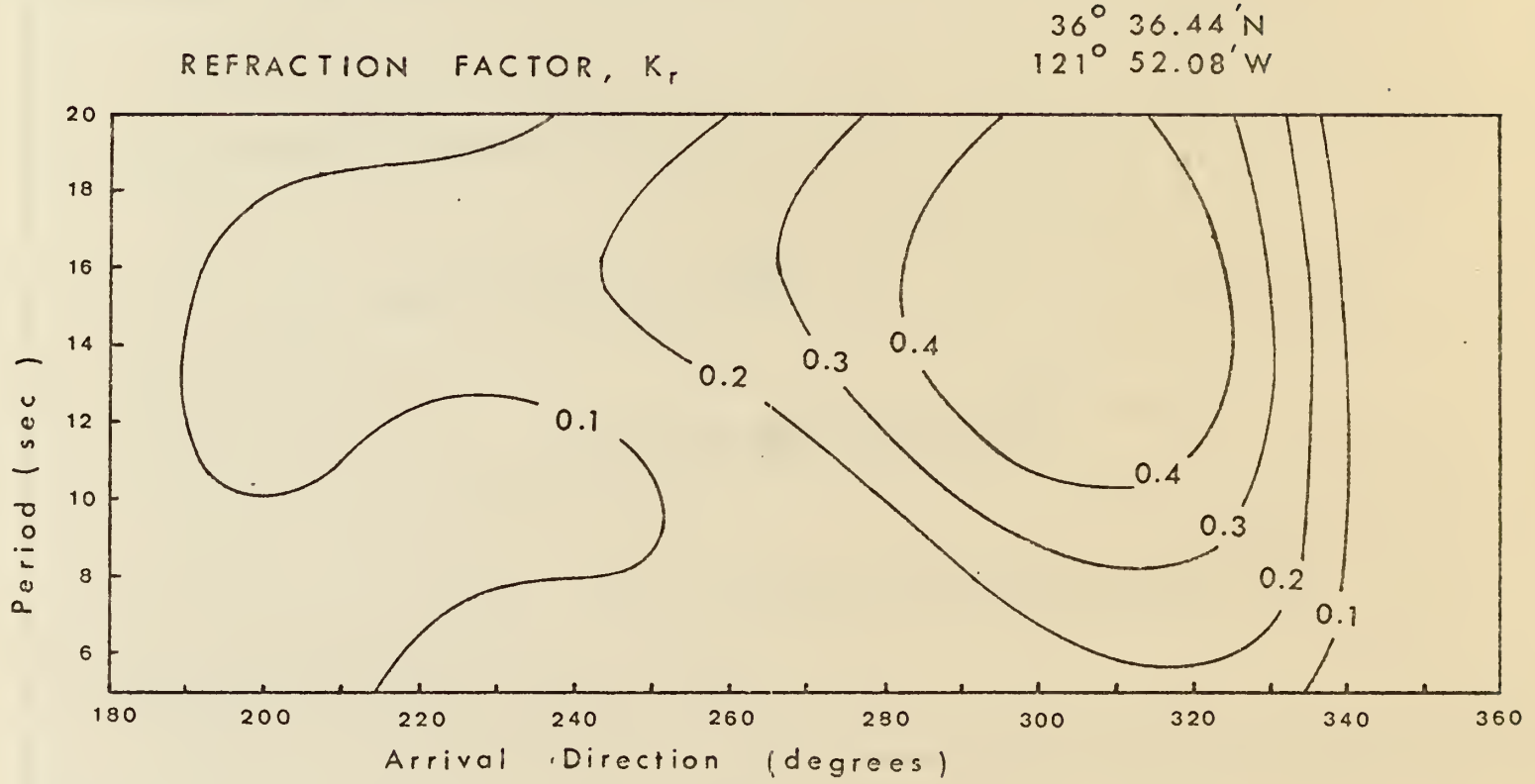

Figure 23: Refraction Graph for Del Monte Beach Sensor Site

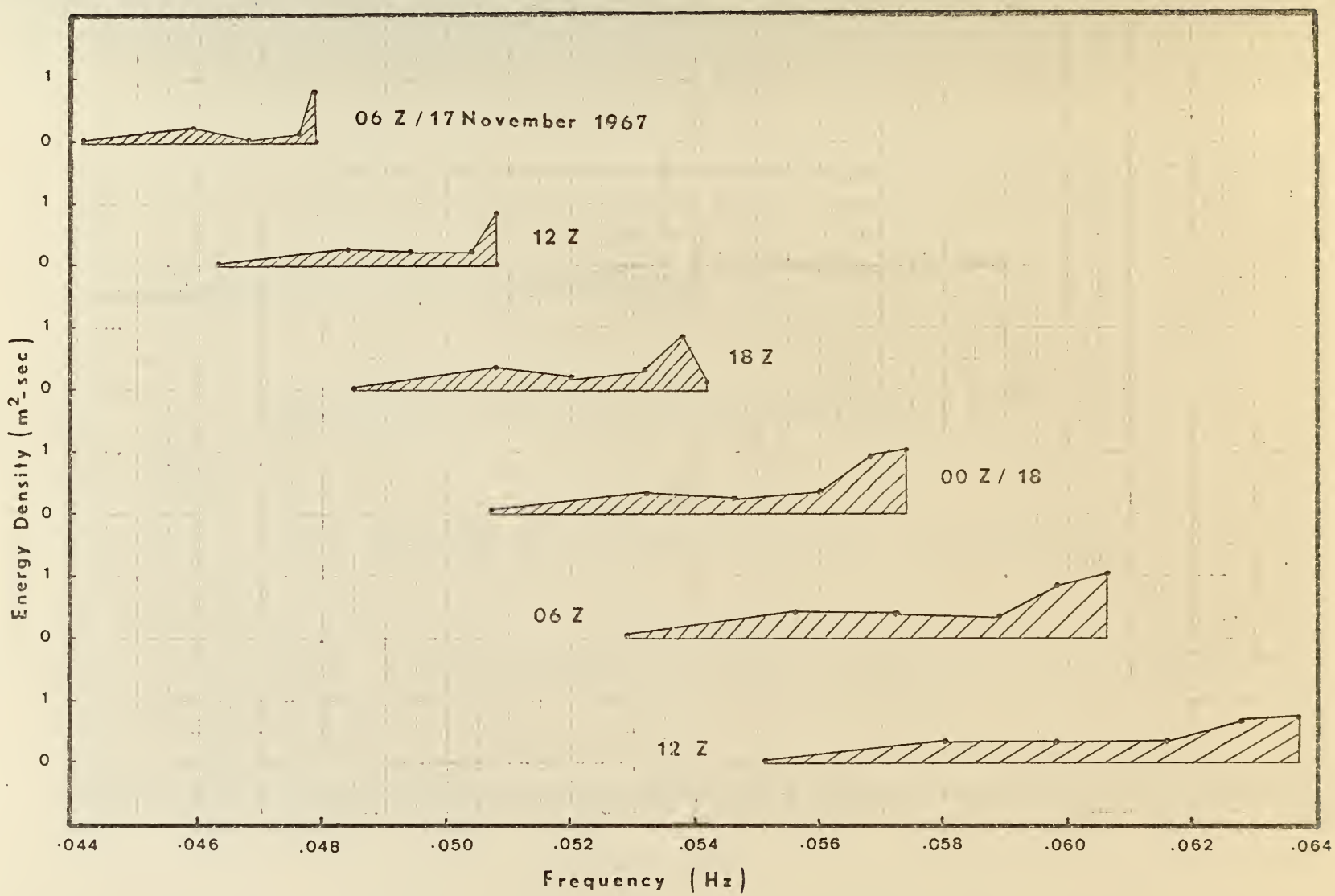

Figure 24: Predicted Shoal Water Swell Energy Spectra for Swell Train 3

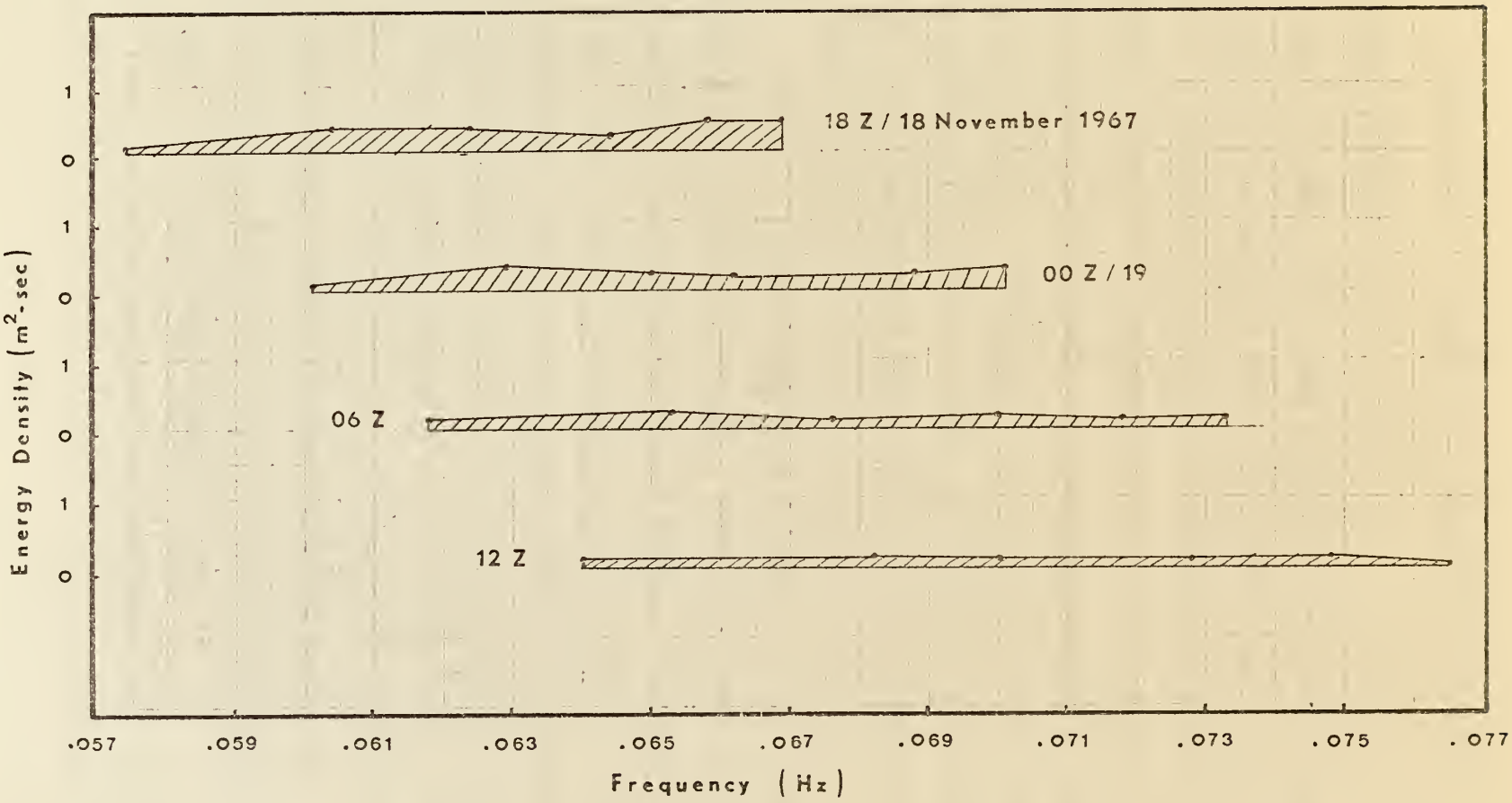

Figure 24: (Continued)

III. COMPARISON OF PREDICTED AND OBSERVED SWELL

A. OBSERVED WAVE DATA

The observed wave data used in this study for comparison with the computed wave data were obtained from analysis of strip-chart recordings from two bottom-mounted pressure-type wave sensors located in approximately 30 feet of water. The strip-chart records from both sensors were manually analyzed by Professor Warren C. Thompson. Wave periods were obtained using the wave-group method, which for distant swell has been shown to yield periods equivalent to the periods of maximum energy density obtained by spectral analysis (Thompson, 1973). The wave records exhibiting the swell originating from Storms 1 through 4 were obtained from the Monterey sensor located at Del Monte Beach. The swell periods from Storm 5 were obtained from a sensor at Stinson Beach, California. The Stinson Beach sensor is located about 75 nautical miles closer to the swell source than the Monterey sensor and approximately on the same great circle trajectory. Since the predicted periods were computed for Monterey, the arrival times of the observed periods recorded at Stinson Beach were adjusted to correspond to arrival times at the Del Monte Beach site.

Significant wave heights at the Monterey gage were determined by adjusting the apparent heights recorded by the pressure gage for the effects of hydrodynamic damping

due to water depth using Wiegel's Tables (Wiegel, 1954). The recorded swell was presumed to be narrow banded so that a single damping factor could be applied with good approximation. The pressure-response factor of the wave gage was greater than 0.988 over the period range from 5 to 20 seconds. The significant wave heights computed from the pressure gage data are referred to as observed heights.

B. SWELL HEIGHT

Significant swell heights at the Monterey gage site were predicted for the swell arriving from two of the storms studied (Storm 1 and Storm 3). Comparisons of predicted and observed signficant heights are shown in Figures 25 and 26. It may be seen that in both sets of swell the observed heights are greater than the predicted heights; in Swell Train 1 the observed heights exceed those predicted by a factor of about 2.6, whereas in Swell Train 3 the factor is about 5. In the case of Swell Train 1, the observed peak height occurred approximately ten hours earlier than predicted. The peak height in Swell Train 3 occurred approximately at the time predicted.

The difference in magnitude between the predicted and observed heights most likely can be attributed to one or more of the procedures used to apply angular spreading, attenuation, and shoaling and refraction. The choice of a 12-millibar interval for defining the fetch width is largely arbitrary and may be too conservative. The way in which the storm limit is defined may have introduced excessive

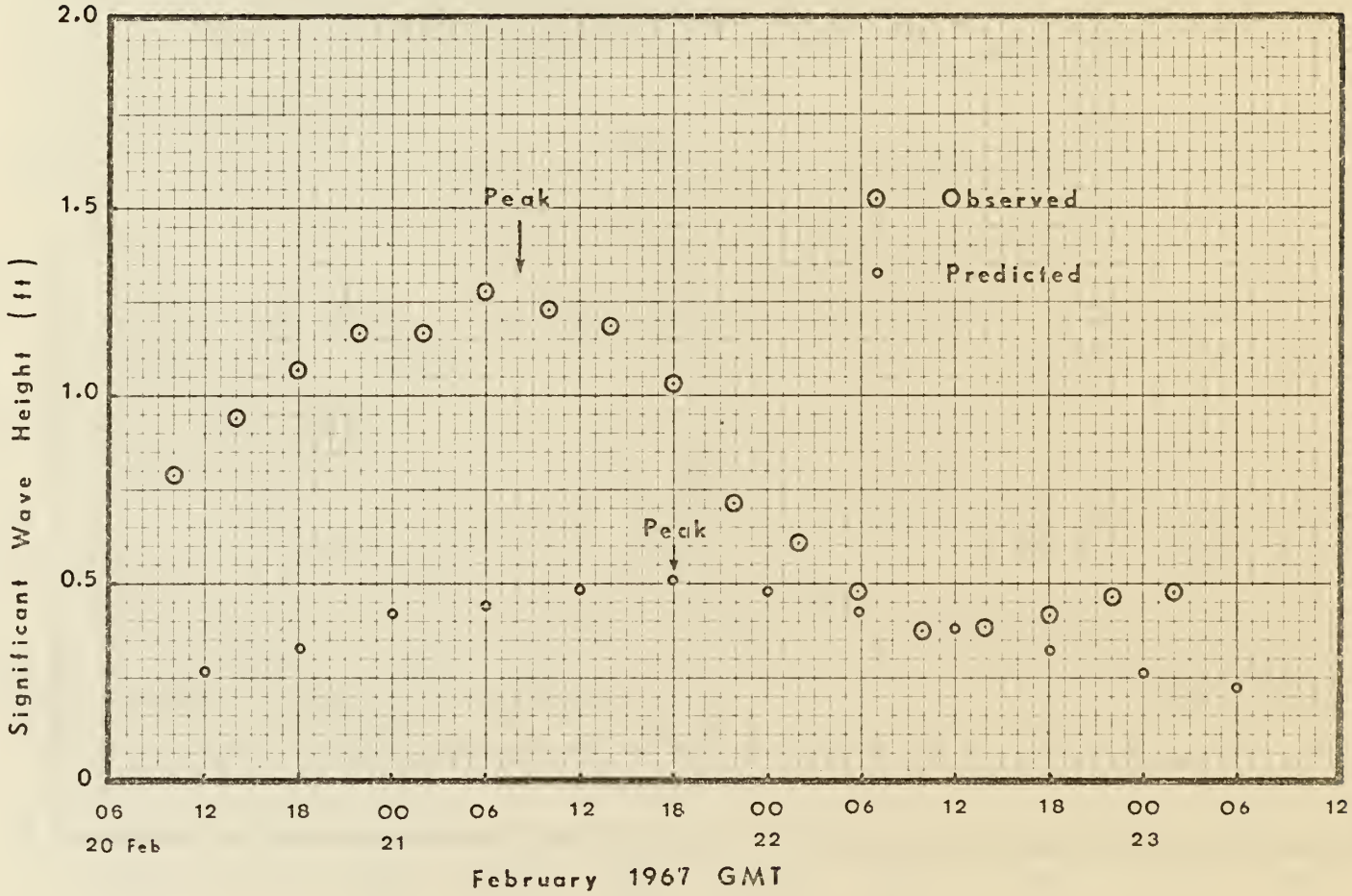

Figure 25: Observed and Predicted Significant Wave Heights for Swell Train 1

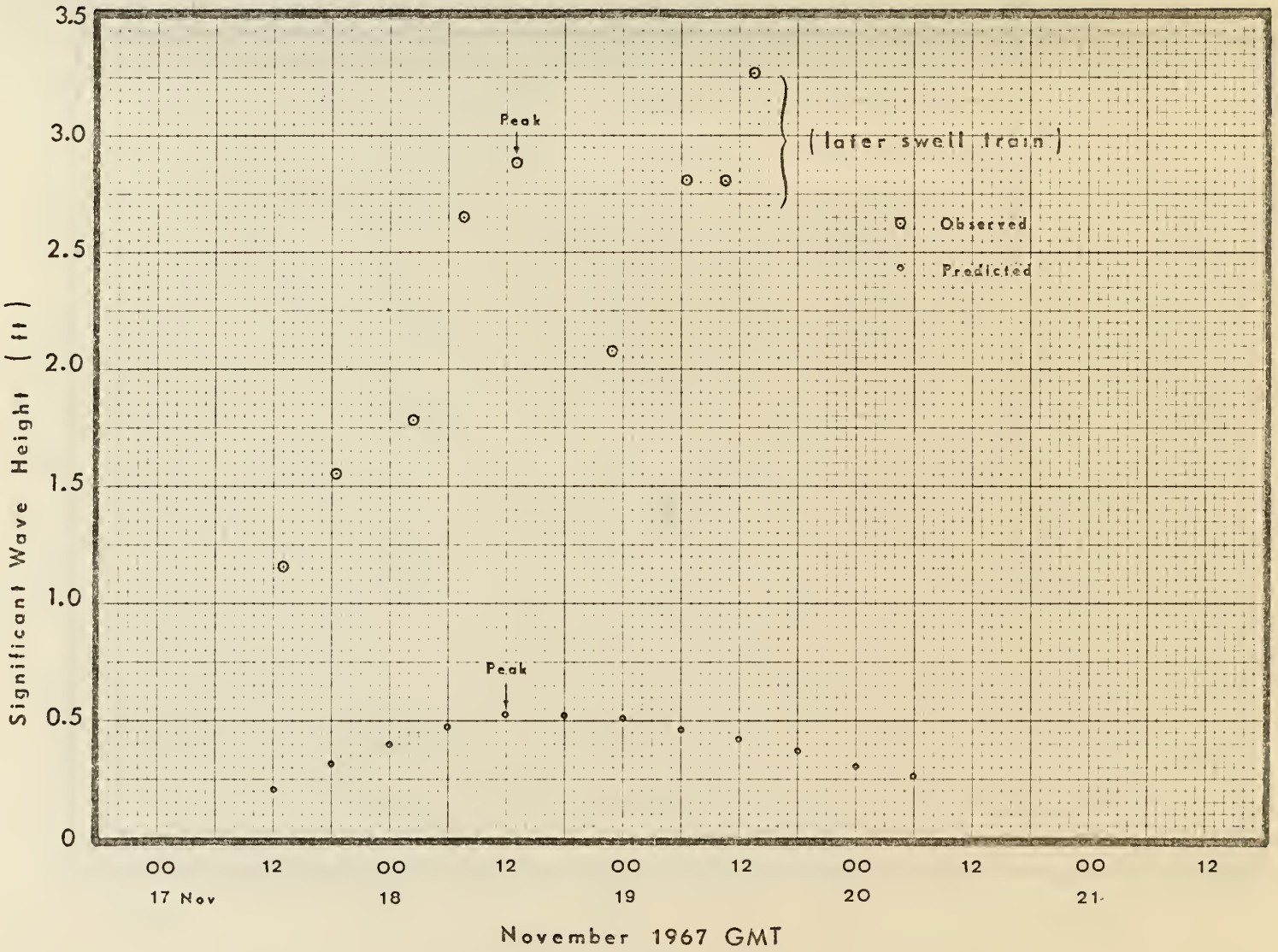

Figure 26: Observed and Predicted Significant Wave Heights for Swell Train 3

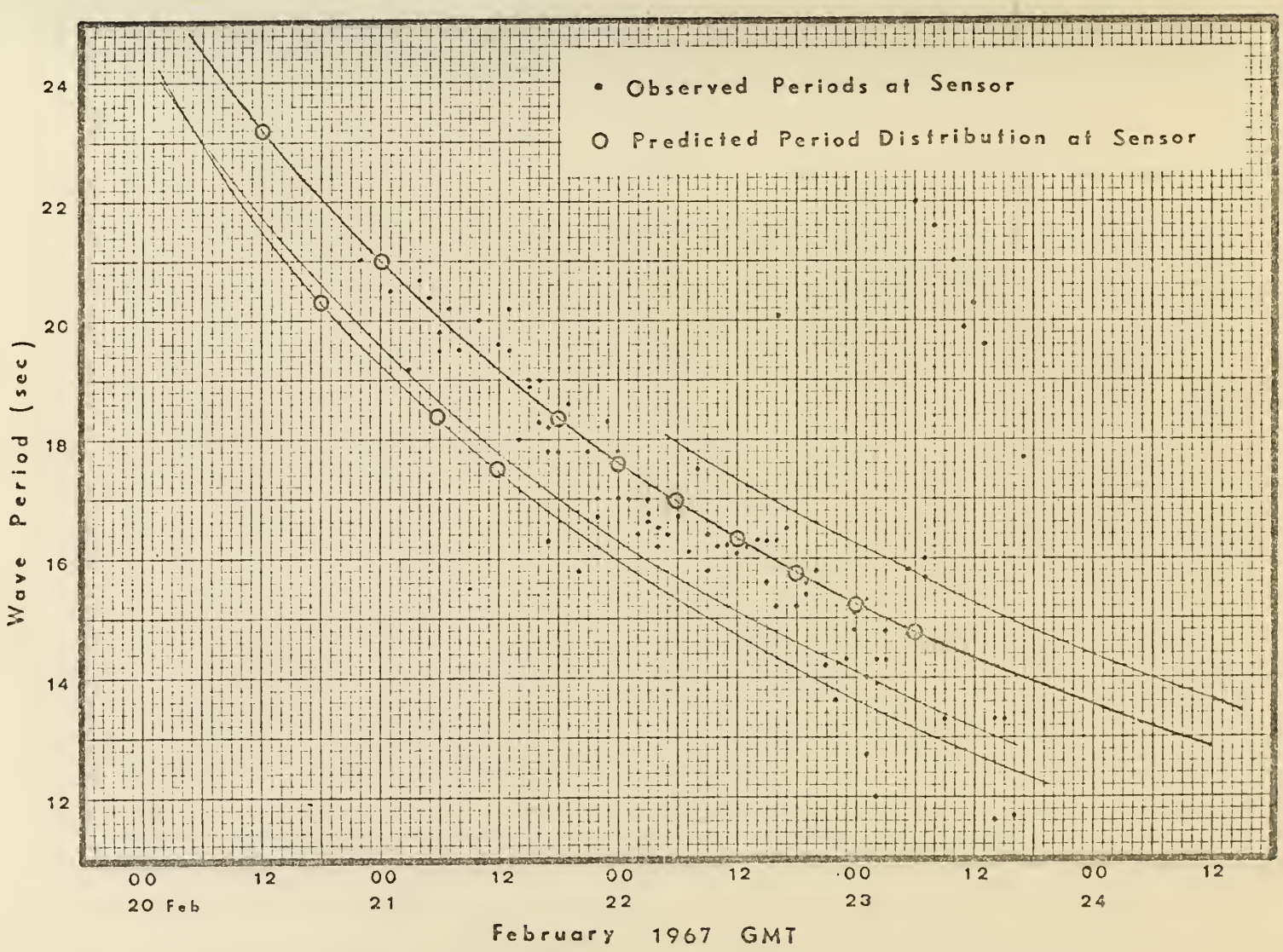

Figure 27: Observed and Predicted Swell Periods from Storm 1

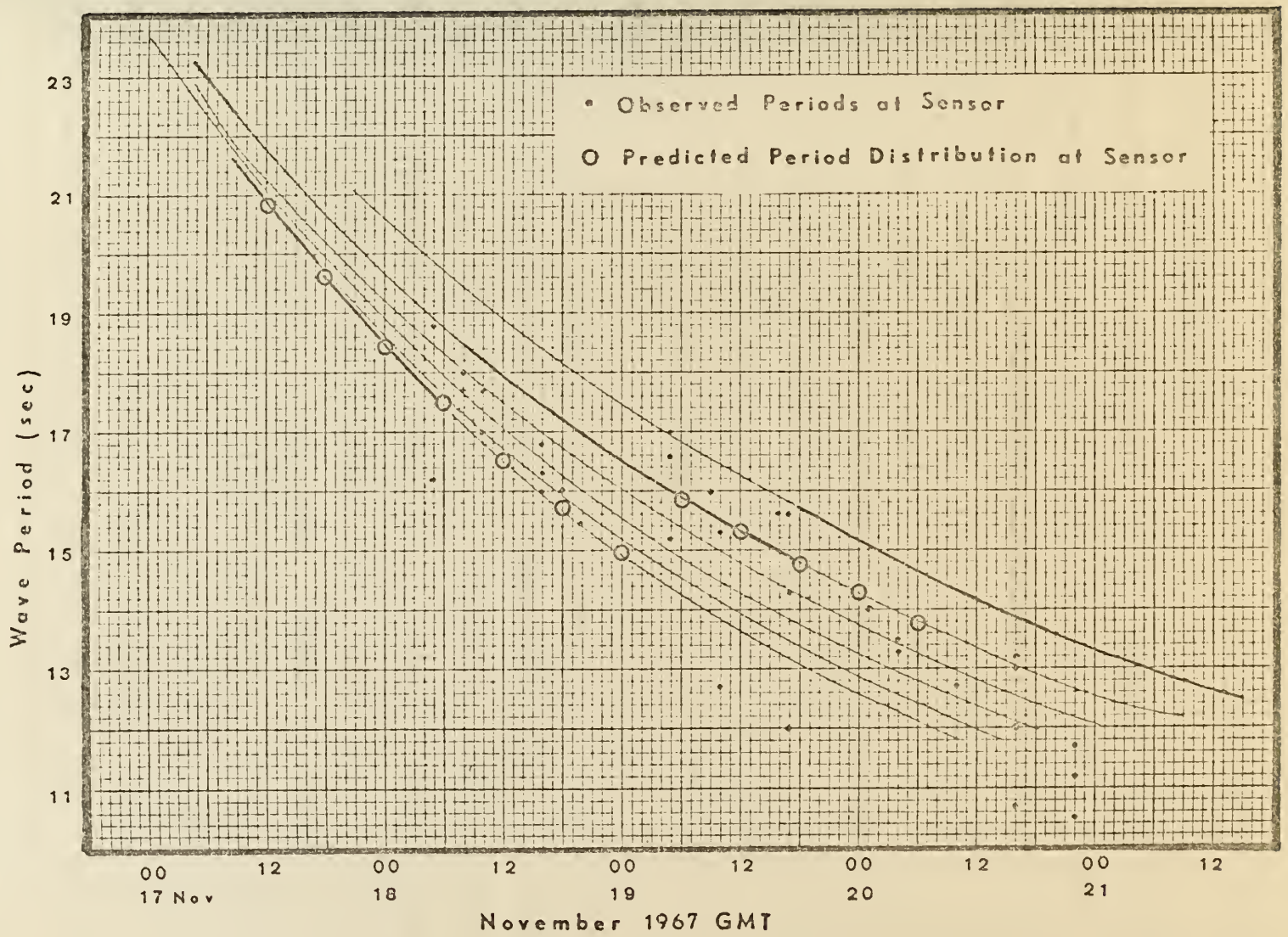

Figure 28: Observed and Predicted Swell Periods from Storm 3

attenuation estimates. Poor refraction data also may have introduced a significant error in the calculations of the shoal-water swell energy.

C. DOMINANT SWELL PERIOD

The distribution with time of the dominant swell period at the wave gage site also was computed for Swell Trains 1 and 3. The results are shown in Figures 27 and 28 by open circles; the observed periods are represented by dots. The predicted and observed periods at the sensor site are superimposed on the family of potential period-time curves computed for Monterey as shown in Figures 4 and 6. As stated earlier, the heavy portions of the period-time curves represent the predicted dominant periods in deep water at Monterey.

In Figure 27 it may be observed, from the predicted period distribution with time in deep water and at the wave gage site, that the shoaling and refraction modifications to the propagated spectra resulted in a shift of the dominant energy from one period-time curve to another in the period band from 18 to 21 seconds. Figure 28 exhibits a similar shift; however, in this case the predicted shift is more consistent with the trend of the observed periods. It may be concluded that the dominant period can shift due to shoaling and refraction, but that the shift is not large. Accordingly, the predicted period-time distributions in deep water are used for comparison with the observed periods at the wave gage for Storms 2, 4, and 5.

Comparison of the period-time distribution of the predicted dominant swell (heavy lines) with the mean trend of the observed periods (dots) for each of the storms (Figures 17 through 21) shows close agreement. For the five storms studied, the mean difference between the predicted and observed periods does not exceed about one second. It may be concluded that the method produces accurate period forecasts.

Differences in the swell-generating characteristics among the five storms may be noted from examination of the predicted periods (heavy lines) and the observed periods (dots) shown in Figures 17 through 21. In Storm 1 (Figure 17), the period-time curve propagated from a single point-source (on the weather chart of 0000Z/16 February 1967) contains the dominant energy over the entire duration of the observed swell at Monterey; this is verified by the close correspondence of the predicted deep-water period distribution with the observed periods. In Storm 4 (Figure 20), the distribution of observed periods also indicates effective generation at a single point-source; however, prediction called for the longest period components of the swell to be generated at the point-source identified on the succeeding weather map, and to arrive sooner. It is evident from an examination of the plot of propagated spectra derived from this storm (Figure 15), that determination of which period-time curve is dominant at a given time is in this case particularly dependent upon the accuracy of the

modifications to the sea spectrum at each point-source due to spectral cutoff, angular spreading, and attenuation.

By contrast, in Storm 3 (Figure 19) there is a noticeable shift of the predicted dominant periods as well as the observed periods from one period-time curve to another such that the dominant energy arriving at different times is propagated from several different point-sources. In Storm 2 (Figure 18), a similar shift in the dominant periods across the dispersion curves may be noted. In this storm, the period-time curves are nearly coincident, which is due to the fact that the speed of the point-source toward Monterey and the group velocity of the peak energy component in each source spectrum were closely coincident. The wide scatter of periods recorded after 0000Z/25 February is attributed to a wave train from another disturbance.

D. REFINED PERIOD PREDICTION

In order to further investigate the apparent shift of the dominant energy from one period-time curve to another, which is particularly apparent in the case of Storm 3 (Figure 19), the synoptic parameters derived from each surface pressure chart (i.e., surface wind speed, storm speed, and distance from the point-source to Monterey) were linearly interpolated at two-hour increments. The period-time distribution of the dominant swell at Monterey obtained from this refined data base is illustrated in Figure 29 by the heavy lines. The associated propagated energy spectra are illustrated in Figure 30. The reader may note that the

time sequence of the dominant segments of the period-time curves reveals the generation history of the arriving swell train. In the period band from 18 to 23 seconds, the dominant energy was generated in the later part of the storm history (1000Z/13 November through 2000Z/13 November); the period band from 13 to 18 seconds was generated early in the storm history (1200Z/12 November through 1800Z/12 November).

The general trend of the dominant periods in the predicted swell may be seen to approximate the trend of the observed periods; however, the correlation does not appear to have been significantly improved by refinement of the six-hourly synoptic data.

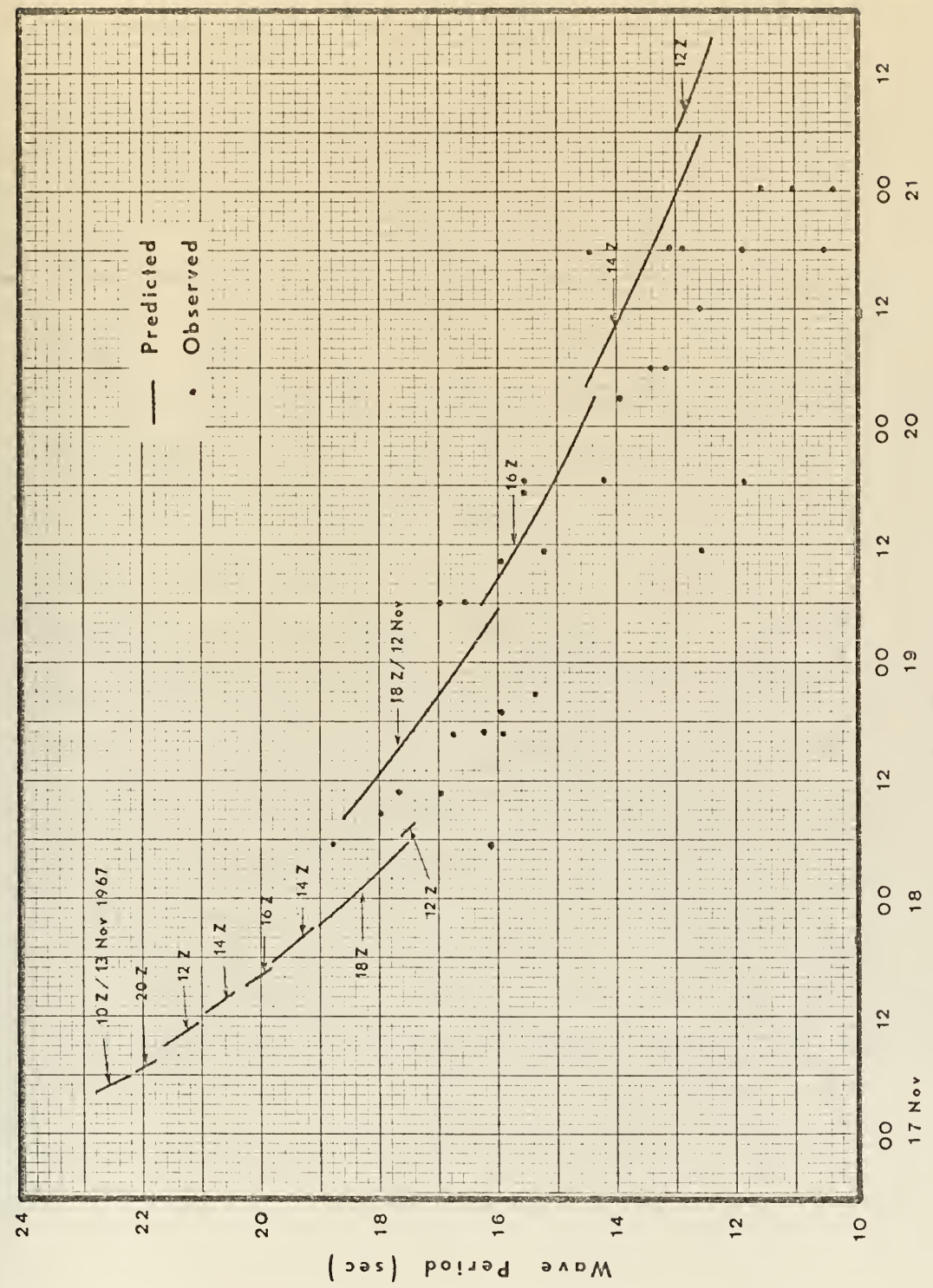

Figure 29: Refined Period Predictions for Swell Train 3

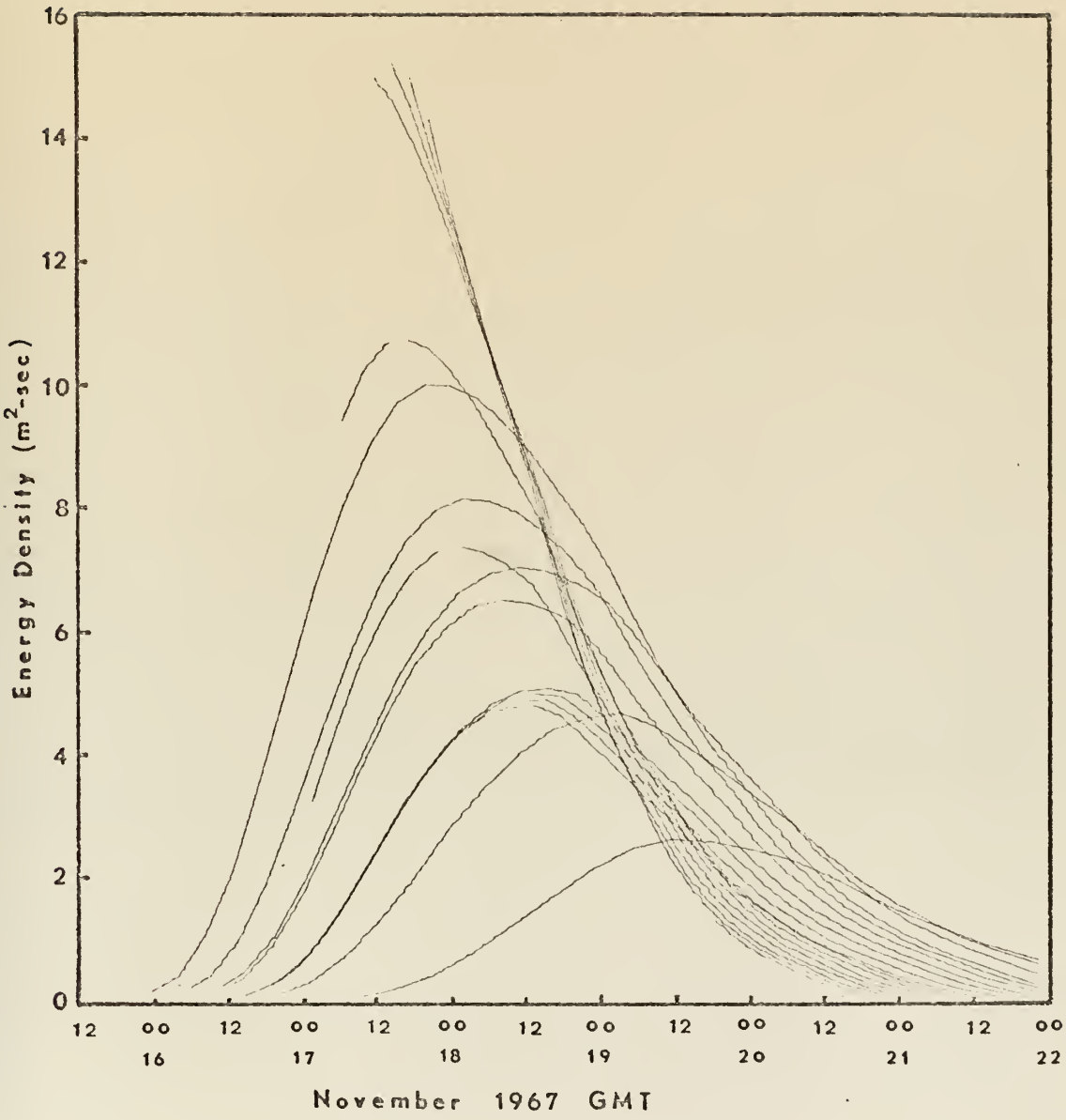

Figure 30: Refined Propagated Spectra from Storm 3

IV. CONCLUSIONS

In spite of the poor height predictions obtained for the two swell trains at the Monterey wave gage site, the multiple point-source method is sufficiently promising with regard to the time of arrival of the maximum swell height and the accuracy of the dominant periods obtained that additional research effort should be expended to test the method further, and to tune the procedures involved so as to give better height predictions. The latter may be accomplished by modifying some of the procedures within realistic limits, particularly the procedures for angular spreading and attenuation. The predicted heights should be compared with observed wave data of better quality than were available in this study, preferably recorded in deep water so that the complications of shoaling and refraction can be eliminated.

LIST OF REFERENCES

1. Braunstein, W. J., 1970. Origin of Swell Recorded at Monterey, California. Naval Postgraduate School, Monterey, California, M.S. Thesis, 74 pp.

2. Bretschneider, C. L., 1963. A One-dimensional Gravity Wave Spectrum. Proceedings of Conference on Ocean Wave Spectra, Prentice-Hall, 357 pp.

3. Carstensen, L. P., 1967. Some Effects of Sea-Air Temperature Difference, Latitude and Other Factors on Surface Wind-Geostrophic Wind Ratio and Deflection Angle. Fleet Numerical Weather Central, Technical Report 29, 9 pp.

4. Hasselmann, K., 1963. On the Non-linear Energy Transfer in a Wave Spectrum. Proceedings of Conference on Ocean Wave Spectra, Prentice-Hall, 357 pp.

5. Kinsman, B., 1965. Wind Waves, Their Generation and Propagation on the Ocean Surface. Prentice-Hall, 636 pp.

6. Longuet-Higgins, M. S., 1952. On the Statistical Distribution of the Heights of Sea Waves. Journal of Marine Research, V. 11, No. 3, p. 245-266.

7. Moskowitz, L., 1963. Estimates of the Power Spectra for Wind Speeds of 20 to 40 Knots. New York University, Department of Meteorology and Oceanography, Geophysical Sciences Laboratory Report 63-11, 39 pp.

8. Munk, W. H., and others, 1963. Directional Recording of Swell from Distant Storms. Philosophical Transactions, Royal Society of London, V. 255, No. 1062, p. 505-584.

9. Neumann, G., 1953. On Ocean Wave Spectra and a New Method of Forecasting Wind-Generated Sea. Corps of Engineers, Beach Erosion Board, Technical Memorandum 43, 41 pp.

10. Phillips, O. M., 1963. The Dynamics of Random Finite Amplitude Gravity Waves. Proceedings on Conference on Ocean Wave Spectra, Prentice-Hall, 357 pp.

11. Pierson, W. J., and L. Moskowitz, 1964. A Proposed Spectral Form for Fully Developed Wind Seas Based on the Similarity Theory of S. A. Kitaigorodskii. Journal of Geophysical Research, V. 69, No. 24, p. 5181-5190.

12. Pierson, W. J., G. Neumann, and R. W. James, 1955. Practical Methods for Observing and Forecasting Ocean Waves by Means of Wave Spectra and Statistics. Naval Oceanographic Office, H. O. Pub. 603, 284 pp.

13. Snodgrass, F. E., and others, 1966. Propagation of Ocean Swell Across the Pacific. Philosophical Transactions, Royal Society of London, V. 259, No. 1103, p. 431-497.

14. Thompson, W. C., 1973. Period by the Wave-Group Method. American Society of Civil Engineers, Proceedings of 13th Coastal Engineering Conference. (In Press).

15. Wiegel, R. L., 1954. Gravity Waves Tables of Functions. Council on Wave Research, The Engineering Foundation, 30 pp.

INITIAL DISTRIBUTION LIST

		No. Copies
1.	Defense Documentation Center Cameron Station Alexandria, Virginia 22314	2
2.	Library, Code 0212 Naval Postgraduate School Monterey, California 93940	2
3.	Professor Warren C. Thompson Department of Oceanography Naval Postgraduate School Monterey, California 93940	5
4.	Lieutenant C. F. Kauffmann USS Marathon (PG-89) c/o FPO San Francisco 96601	2
5.	Professor J. B. Wickham Department of Oceanography Naval Postgraduate School Monterey, California 93940	1
6.	Department of Oceanography Naval Postgraduate School Monterey, California 93940	3
7.	Lieutenant Commander Charles K. Roberts Department of Oceanography Naval Postgraduate School Monterey, California 93940	1
8.	Oceanographer of the Navy The Madison Building 732 N. Washington Street Alexandria, Virginia 22314	1
9.	Dr. Ned A. Ostenso Code 480D Office of Naval Research Arlington, Virginia 22217	1
10.	Evelyn L. Pruitt, Director Geography Programs, Code 414 Office of Naval Research Department of the Navy Washington, D. C. 20360	1

11. Commanding Officer — 1
Environmental Prediction Research Facility
404 Franklin Street
Monterey, California 93940

12. Commanding Officer — 2
Fleet Numerical Weather Central
Monterey, California 93940

13. Coastal Engineering Research Center — 1
5201 Little Falls Road, N. W.
Washington, D. C. 20016

14. Mr. Charles Fisher, Chief — 1
Coastal Engineering Branch
U. S. Army Corps of Engineers
P. O. Box 2711
Los Angeles, California 90053

15. Commanding Officer — 2
San Francisco District
U. S. Army Corps of Engineers
100 McAllister Street
San Francisco, California 94102
Navigation and Shoreline Planning Section
Library

16. Coastal Engineering Branch — 1
Planning Division
U. S. Army Engineering Division, South Pacific
630 Sansome Street
San Francisco, California 94111

17. Dr. D. Lee Harris — 1
Coastal Engineering Research Center
5201 Little Falls Road, N. W.
Washington, D. C. 20016

18. Mr. Richard W. James — 1
Code 77
Naval Oceanographic Office
Washington, D. C. 20390

19. Dr. Peter Badgley — 1
Code 410
Office of Naval Research
Naval Research Laboratory
Arlington, Virginia 22217

UNCLASSIFIED
Security Classification

DOCUMENT CONTROL DATA - R & D

(Security classification of title, body of abstract and indexing annotation must be entered when the overall report is classified)

ORIGINATING ACTIVITY (Corporate author)

Naval Postgraduate School
Monterey, California 93940

2a. REPORT SECURITY CLASSIFICATION

Unclassified

2b. GROUP

REPORT TITLE

SWELL PREDICTION BY A MULTIPLE POINT-SOURCE SWELL GENERATION MODEL

DESCRIPTIVE NOTES (Type of report and inclusive dates)

Master's Thesis; March 1973

AUTHOR(S) (First name, middle initial, last name)

CARL F. KAUFFMANN

REPORT DATE	7a. TOTAL NO. OF PAGES	7b. NO. OF REFS
March 1973	73	15

8a. CONTRACT OR GRANT NO.	9a. ORIGINATOR'S REPORT NUMBER(S)
b. PROJECT NO.	
c.	9b. OTHER REPORT NO(S) (Any other numbers that may be assigned this report)
d.	

10. DISTRIBUTION STATEMENT

Approved for public release; distribution unlimited.

11. SUPPLEMENTARY NOTES	12. SPONSORING MILITARY ACTIVITY
	Naval Postgraduate School Monterey, California 93940

13. ABSTRACT

A method was developed for forecasting swell using a spectral wave-generation model based on a multiple point-source concept of swell origin. The multiple point-source concept considers that the peak-energy swell emanating from a moving cyclonic storm can be considered to have been produced at one or more space-time point sources in the storm by the impulsive introduction of energy into the sea. The method was tested on five North Pacific storms generating swell recorded at Monterey, California. Predicted swell heights, which were made for two storms, were significantly lower than the observed heights. The time of occurrence of the predicted peak height agreed with that observed for the swell from one storm, but differed by about ten hours for the other. Predictions of the dominant swell period were accurate to within about one second over the entire range of observed periods for all storms.

DD FORM 1 NOV 68 1473 (PAGE 1)
S/N 0101-807-6811

UNCLASSIFIED
Security Classification

A-31408

14 KEY WORDS	LINK A		LINK B		LINK C	
	ROLE	WT	ROLE	WT	ROLE	WT
Swell Origin						
Swell Prediction						
Swell Propagation						
Wave Forecasting						
Wave Attenuation						